UNIVERSITY OF GENOVA

PHD PROGRAM IN BIOENGINEERING AND ROBOTICS

Force-Torque Sensing in Robotics

by

Francisco Javier Andrade Chavez

Thesis submitted for the degree of *Doctor of Philosophy* (31° cycle)

December 2018

Francesco Nori	Supervisor
Daniele Pucci	Supervisor
Silvio Traversaro	Co-Supervisor
Giorgio Cannata	Head of the PhD program

Thesis Jury:

Olivier Stasse, *Directeur de Recherche CNRS at LAAS, Toulousse*	External examiner
Andrea Del Prete, *Tenure-track assistant professor at University of Trento*	External examiner
Matteo Fumagalli, *Associate Professor at Aalborg University Copenhagen*	External examiner

Dibris

Department of Informatics, Bioengineering,
Robotics and Systems Engineering

iit DIC
ISTITUTO ITALIANO
DI TECNOLOGIA

Dynamic Interaction Control Lab

I would like to dedicate this thesis to my family that has always believed in me and supported me in any way they can even from afar. To my parents, my sister, grandmas, uncles, aunts, and cousins I love you all. Of course, I dedicate this work also to my wife who brings me joy and is always there with me and for me when I need her. She boarded in the boat of my craziness and has not turned back. For this and many many other things you are my place to be, my home sweet home and my love sweet love. But most especially to my son Francisco Gabriel who changed my life more than I could have changed it myself. Whom would not let me work in his presence while motivating me to work harder, better, and faster with his bare existence. I will strive to give you the opportunity of doing what you love as I do. To you more than anyone I dedicate this thesis including this:

" You are the chaos that brought order to my life.
Of course, I knew I wanted you this bad.
That is why I feared you so hard.
I knew you would change my body, soul and mind.
And now you are here, crushing every escape.
Now I'm trapped because I hope you will hold me forever in your hands.
You hacked my brain, turn upside down my nights,
having me not knowing if I'm awake, hungry or what.
But it all makes sense and its worth every drop of sweat,
when you hold my hand, fall asleep in my lap
or give me the precious gift of your smile.
I'm here to stay, hoping to hear you tell me whatever you want.
Cause from now on I exist to ensure you get a beautiful life.
I am from now to eternity your dad
and there is no way I would have ever changed that. "

Your Dad.

Acknowledgements

I would like to acknowledge Universita degli studi di Genova for the opportunities they have given in these three years. To the National Council of Science and Technology (CONACYT) in Mexico for their support ever since the Master. To the Dynamic Interaction Control lab who took me in and help me grow as a researcher.
I would like to acknowledge as well the people from iCub facility that where there every time I needed something with a welcoming attitude. I would like to acknowledge especially the help of Silvio Traversaro, Gabriele Nava, Nuno Guedelha, and Luca Fiorio. Their help made my research life much easier and I would dare say possible. A special acknowledgment for Francesco Nori who decided I was a good candidate for the lab and to Daniele Pucci for letting me pursue my ideas while motivating me to keep up the good work.
For different reasons but just as important I would like to acknowledge all the people I have met during these three years. They made my life here rich in experiences and fun. Especially to the Team Tequila and the Mexican Mafia group, you guys are my family here.

Abstract

Being able to perform dynamic motions repeatably and reliably is an active research topic. The present thesis aims to contribute to this by improving the accuracy of force-torque sensing in robots. It focuses primarily on six axis force-torque sensors, although other sources of force-torque sensing are explored. Force sensing technologies, calibration procedures of these sensors and the use of force-torque sensing in robotics are described with the aim to familiarize the reader with the problem to solve. The problem is tackled in two ways: improving the accuracy of six axis force-torque sensors and exploring the use of tactile sensor arrays as force-torque sensors. The contributions of this thesis are : the development of the Model Based In situ calibration method for improving measurements of sensors already mounted on robots and the improvement in performance of the robot as a consequence; the design of a calibration device to improve the reliability and speed of calibration; and the improvement of force sensing information of a capacitive tactile array and its use on a robot as force-torque information source. The developed algorithms were tested on the humanoid robotic platform iCub.

Prologue

Robots are expected to perform highly dynamical motions. Being able to perform these motions repeatably and reliably is an active research topic. Achieving this type of motions requires information of the interaction forces that exist whenever a contact is established. This thesis aims to help to research this type of motions by enriching the quality of the information obtained during this kind of behaviors, more specifically force related quantities.

Science fiction has given us a lot of expectations in what a robot should look like and be able to do. It is not uncommon to see a robot walk, run, jump and even parkour in movies and cartoons. There are in fact some videos of actual robots starting to reach some of these dynamic behaviors. But in reality, we are far from reaching a point where a robot can move around in a reliable way. As mentioned by Boston Dynamic's CEO Marc Raibert, "In our videos we typically show the very best behavior. It's not the average behavior or typical behavior. And we think of it as an aspirational target for what the robots do."

A crucial part of these motions is the interaction of the robot with other objects or the environment. Whenever an interaction happens there exist an exchange of forces. As humans, we are only able to walk thanks to the gravity force keeping us anchored to the ground and the friction forces allowing us to propel forward.

A robot, as the machine that it is, bases its behavior on programmed responses to perceived stimulus. Independently of how the behavior is programmed a considerable part of the reliability comes from the perceived stimulus. When the stimulus is limited to a start command the behavior is executed in feedforward. In this way, the robot has no way of understanding if it has full filled its goal or not. By giving relevant information to the robot it is possible to create a self-correcting action to achieve the desired behavior. This relevant information is called feedback.

The nature of what is considered relevant information depends on the nature of the behavior involved. As mentioned, whenever there is an interaction with other objects or the environment there exist forces. It is then straight forward to see that knowledge about the exchanged forces is relevant information for dynamic behaviors.

Force-torque sensing is the ability to sense or measure the forces and torques exchanged

between two objects. There are mainly two interesting force sensing quantities for robots, the joint torques, and the contact forces.
The joint torques have a direct relationship with the output of the motors at the joints. Therefore, joint torques are relevant information for programming the behavior of the motors. This is usually done through joint torque controllers that benefit greatly from using joint torque values as feedback.
On the other hand, contact forces are the actual forces and torques exchanged at the contact location when an interaction between objects is happening. This information has a direct relationship with the effect an object can have on another object or in itself by exploiting the contact.
To measure this quantities many different kinds of sensors have been developed. A sensor is a device that receives a stimulus and responds with an electrical signal [43]. Based on the type and amount of forces that they measure, force sensors can be classified in single-axis force sensor, single-axis torque sensor, and multi-axis force-torque sensor. These sensors are typically placed near the place in the robot where the information might be more useful. For single-axis torque sensors, a common location is near the joints to provide direct feedback on the joint torque. For single-axis force sensors and multi-axis force-torque sensors, the location is usually near the end effectors to measure the contact forces. A special type of multi-axis force-torque sensors are the six axis force-torque (FT) sensors which convey a complete information of a contact force by providing measurements of the three axes of forces and three axes of torques.
A force sensor does not measure the force directly. Measuring a force is the result of converting other physical phenomena that varies in response to force into an electrical signal. The relationship between the change of the phenomena to an actual force value is obtained through a process called calibration. The accuracy of the sensor is then a result of the calibration process. It requires the mathematical model of the phenomena (or a good approximation) and known stimuli paired with the corresponding sensor's response.
The most common phenomena used in force-torque sensors is the change in resistance of silicon due to strain. In more technical words, the piezoresistive response to strain of semiconductor material. This material also changes resistance with temperature. Because of this, depending on the calibration procedure, the sensor might suffer from temperature drift. Temperature drift is defined as the undesired change of measurement due to changes in temperature.
Tactile sensors are based on similar phenomena used for force-torque sensors. But, since the main objective of tactile sensors is the detection of contact and not the measuring of force, they are not accurate enough to be directly used as force-torque sensors. The accuracy required for using them as force-torque sensors might be achieved with the proper calibration procedure.
A pair of known stimuli with the sensor response is called a calibration point. A set of cal-

ibration points is a calibration data set. In this thesis, calibration procedures are classified depending on the place the calibration data set is acquired. If the calibration data set is acquired in the system (or structure) in which is meant to be used, it is referred to as *in situ* calibration. Instead, if the sensor is calibrated in a structure then removed and mounted somewhere else for its use, it is referred to as *ex situ* calibration.

In standard operating conditions, a decrease in the effectiveness of the calibration may occur in months. Leading companies for force-torque (FT) sensors [11, 142] recommend calibrating the sensors at least once a year. The calibration done by the manufacturer is typically an *ex situ* calibration. As such, it usually implies that the sensor must be unmounted, sent back to them, calibrate the sensor in a special setup, receive the sensor again and then mount it.

FT sensors are prone to change performance once mounted in a mechanical structure such as a robot [130, 8]. Different methods have been developed to re-calibrate the sensors once mounted. These *in situ* calibration methods allow to perform the calibration in the sensor's final destination, avoiding the decrease in performance that arises from mounting and removing the sensors from its working structure. The relevance of calibrating *in situ* has become evident, making *in situ* calibration part of the service provided by some FT sensor companies [71].

At present, robots still struggle with handling unexpected interactions with their environment, as it could be observed at the DARPA Robotics Challenge Finals in June 2015 [32]. During the challenge, most of the teams could not take advantage of having FT sensors. The Boston Dynamics ATLAS' six axis FT sensors were not used or fully exploited due to the bad quality of sensors measurements, to the point that the IHMC and MIT teams used the FT sensors only as binary contact sensors.

Therefore the objective of this thesis is to provide the knowledge and algorithms needed to have a reliable and accurate estimation of contact forces and joint torques exchanged between the robot, the environment, and other objects. It focuses on improving the measurement reliability of the six axis FT sensors. This allowed robots to perform better dynamical motions. This was achieved by developing novel *in-situ* calibration methods and proposing a new *ex situ* calibration device. Other sources of force-torque information, such as tactile arrays, were explored. This should enable the research community to better exploit force-torque sensing in complex structures such as robots.

There are three intermediate goals to achieve the general objective previously described:

1. Deep understanding of force-torque (FT) sensors.
2. Improvement of force-torque sensors' performance.
3. Increase performance of dynamical motions in robots through the use of force-torque sensing.

To gain a deep understanding of the FT sensors the following actions were taken:

- Study the functioning principles of the different six axis FT sensing technologies.
- Understand how force-torque sensing is used in robots.
- Investigate how six axis FT sensors are usually calibrated.
- Analyze the performance of six axis FT sensors mounted on robots.

Seeking to improve force-torque sensors' performance the strategies implemented were:

- Development of *in-situ* calibration methods.
- Design of an improved *ex-situ* calibration method.
- Investigate the feasibility of using tactile sensors as force-torque sensors.

Aiming to increase the performance of dynamical motions in robots through the use of force-torque sensing, it was considered necessary to:

- Allow the articulated body to exploit the improved measurements.
- Evaluate the result of improving measurement quality.
- Allow the possibility to exploit other sources of force-torque information, such as tactile sensor arrays.
- Allow the robot to estimate individually forces when more than one force is acting on the same robot.

What follows is a brief summary of the thesis structure. It can broadly be considered to be divided into two parts. One is the accumulation of knowledge deemed necessary to achieve the objectives. The other is the result of the research carried out during the last three years in a collaborative Ph.D. between Istituto Italiano di Tecnologia and Universita degli studi di Genova.

Chapters belonging to part one are:

- Chapter 1 seeks to provide information on the force sensing technologies starting from the principles of measuring force to the most common technologies used in six axis force-torque sensors. The available commercial options for robots are presented in a small survey of commercial solutions. Finally, the general use of force-torque sensing in robotics is depicted.

- Chapter 2 describes the use of force-torque sensing in robotics. A method to exploit the force-torque sensing for estimating joint torques and contact forces is detailed. The current performance of robots doing dynamic motions is also depicted.

- Chapter 3 describes what is calibration. It also shows the models used to calibrate six axis FT sensors and capacitive tactile sensor arrays. Some examples of different calibration procedures both *ex situ* and *in situ* are mentioned. It also describes the reasons behind the presented research and the conditions in which it can be applied.

The chapters belonging to the second part are:

- Chapter 4 aims to provide a detailed description of the tools developed to evaluate the performance of a six axis FT sensors once it is mounted on a robot. This is followed by the results of some tests using the aforementioned tools and a description of typical issues that arise when using these type of sensors.

- Chapter 5 displays improvements in the measurements of six axis FT sensors through *in situ* calibration. An algorithm taking advantage of the knowledge of the robot model was developed to perform *in situ* calibration. A detailed description of the calibration algorithm and the results are shown. This is the main work of the thesis, since improving the measurements of the sensor while mounted on the robot, leads to a direct impact on its performance.

- Chapter 6 presents an alternative solution to the current *ex situ* calibration of the lab, based on insights gained from the *in situ* algorithms. The current calibration method is also described and compared to some extent with the proposed solution.

- Chapter 7 explores the possibility of using the skin as a FT sensor. Algorithms to estimate contact locations, external forces, and joint torques using distributed tactile sensor arrays (artificial skin), kinematic sensors and a single IMU without the need for force-torque sensors are presented.

- Chapter 8 confronts the results with the objectives and mentions the future work.

Some of the results contained in this thesis have been or are about to be published in research papers [8, 7, 6].

Table of contents

List of figures

List of tables

Chapter 1

Force-torque Sensing

The main reference for the relation between motion and forces are the three Newton laws of motion. These laws are:

1. Every object in a state of uniform motion tends to remain in that state of motion unless an external force is applied to it.

2. Force is equal to the change in momentum per change in time. For a constant mass, this is:

$$F = ma, \tag{1.1}$$

   where m (kg) is an object's mass, a ($\frac{\mathrm{m}}{\mathrm{s}^2}$) its acceleration and F (N) the applied force.

3. For every action, there is an equal and opposite reaction.

The second law is the most powerful of Newton's three Laws because it allows quantitative calculations of dynamics. Motion involves actions and interactions of a variety of forces. Given the intrinsic relationship between motion and forces, no measurement is more fundamental to understand and perform dynamical motions than the measurement of force and force related quantities (mass, acceleration, pressure, etc). Force sensing is the ability to sense or measure the forces exchanged between two objects. The system that performs the force sensing is a force sensor. A sensor is a device that receives a stimulus and responds with an electrical signal [43]. Force-torque sensing is a special kind of force sensing, it is described as the ability to sense or measure the forces and torques exchanged between two objects. It allows to have a complete description of the sum all of forces and torques between the two bodies at the location where the contact is happening.

In this Chapter, the different technologies used in force sensing are described as well as the principles in which they are based on.

1.1 Force Sensing Technologies

An unknown force can be measured using one of the following means [31]:

1. Balancing it against the known gravitational force on a standard mass, either directly or through a system of levers.
2. Measuring the acceleration of a body of known mass to which the unknown force is applied.
3. Balancing it against a magnetic force developed by the interaction of a current carrying coil and a magnet.
4. Transducing the force to a fluid pressure and then measuring the pressure.
5. Applying the force to some elastic member and measuring the resulting deflection.
6. Measuring the change in precession of a gyroscope caused by an applied torque related to the measured force
7. Measuring the change in natural frequency of a wire tensioned by the force.

All the previously described force sensing methods are mainly applied to static or slowly varying loads. The method number 5 is widely used for both static and dynamic loads of frequency up to many thousand hertz. Sensors based on method 5 are essentially spring-mass systems with damping. They differ in the geometric form of "spring" employed and in the transducer used to obtain an electrical signal. In modern sensors, the most commonly used method is 5, while 3 and 4 are used occasionally [42].

In many sensors, force is developed in response to some stimulus s. The force is not directly converted into an electric signal, thus some additional steps are usually required. A typical force sensor is a combination of a force-to-displacement transducer and a displacement sensor that converts displacement to an electrical output. In other words, a typical force sensor combines an elastic element (spring, polymer lattice, silicon cantilever, etc.) and a gauge for measuring the degree of the element compression or strain for the purpose of converting it to an electrical output signal E. The trend in modern sensor design focuses on the integration of sensing components with signal conditioning, converting, and communication circuits [43]. Such a combination is called a sensing module, Fig. 1.1. Typical sensing element produces low-level analog signals, its output signals need amplification, filtering, impedance matching, and perhaps a level shifting, before it can be digitized. All these functions are performed by

signal conditioners. After conditioning, the signal is converted to digital data using the analog-to-digital converter (ADC). Although all components of the sensing module are important, the thesis focuses more in detail on the elastic element and the displacement sensor.

Their ability to measure dynamic loads coupled with the possibility of a large measurement bandwidth makes strain gauges, plus some elastic element, the main source of force-torque sensing in robotics.

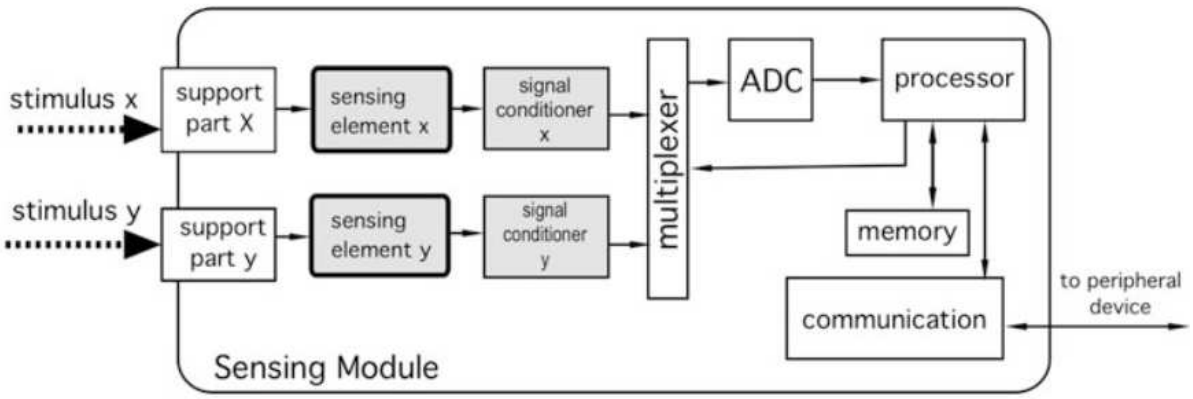

Fig. 1.1 Block diagram of sensing module [43].

1.2 Elastic Element

Elasticity is the ability of an object or material to resume its normal shape after being stretched or compressed. Most materials which possess elasticity in practice remain purely elastic only up to very small deformations. The elastic element is the part of the force sensor that directly responds to the force stimuli.

The relationship between the elastic deformation and forces is given by Hooke's Law. Hooke's law is a law of physics that states:

$$F = k\Delta x, \tag{1.2}$$

where k ($\frac{\mathrm{N}}{\mathrm{m}}$) is a constant of the elastic element, Δx (m) is the change in distance of the elastic element.

Stress σ (Pa) is expressed in terms of force applied to a certain cross-sectional area A (m^2) of an object,

$$\sigma = F/A. \tag{1.3}$$

There are two types of stress depending on the orientation of the force with respect to the cross-sectional area. If the force is perpendicular to the area then it is called normal stress σ_n, Fig. 1.2a. The force can be tensile or compressive depending on the direction of the force. By convention, a compressive force is taken to be negative, which yields a negative stress [20]. Instead, if the force is applied parallel to the cross-sectional area is called shear stress σ_τ. Applying the same stress formula for shear stress results in the average shear stress.

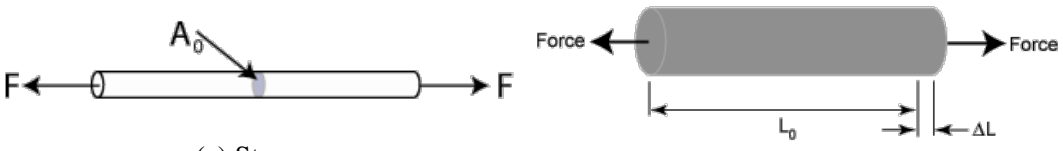

(a) Stress.

(b) Strain.

Fig. 1.2 Effect of a force on a fixed body.

Strain (ε) is the deformation of a physical body under the action of applied forces, Fig. 1.2b. It has no units. Strain is calculated as

$$\varepsilon = \frac{l_i - l_0}{l_0} = \frac{\Delta l}{l_0}, \tag{1.4}$$

where l_0 (m) is the initial length and l_i (m) is length after applying a load. Strains are classified as either normal or shear. A normal strain ε_n is perpendicular to the face of an element, and a shear strain ε_τ is parallel to it. These definitions are consistent with those of normal stress and shear stress.

An object subjected to stress will experience some strain as a result. The relationship between the stress and strain of a particular material is known as the stress-strain curve, Fig. 1.3. It is unique for each material and is found by recording the amount strain at distinct intervals of tensile or compressive stress. The elasticity of materials is described by a stress-strain curve.

An elastic modulus (also known as modulus of elasticity) is a quantity that measures an object's resistance to being deformed elastically (i.e., non-permanently) when a stress is applied to it. The elastic modulus of an object is defined as the slope of its stress-strain curve in the elastic deformation region. A stiffer material will have a higher elastic modulus.

There are various elastic moduli. All of which are measures of the inherent elastic properties of a material as the resistance to deformation under an applied load. The various moduli apply to different kinds of deformation.

Young's modulus E (Pa) is

$$\mathrm{E} = \frac{\sigma_n}{\varepsilon_n} \tag{1.5}$$

, whereas the shear modulus E (Pa) is

$$\mathrm{G} = \frac{\sigma_\tau}{\varepsilon_\tau}. \tag{1.6}$$

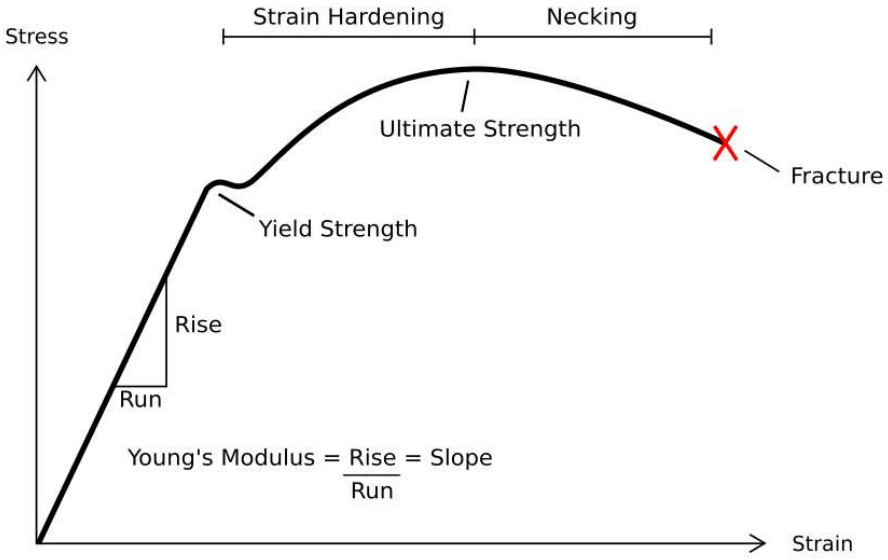

Fig. 1.3 Stress-strain curve.

Hooke's law usually applies to any elastic object, of arbitrary complexity, as long as both the deformation and the stress can be expressed by a single number. Using the elastic moduli, Hooke's law becomes:

$$\sigma_n = \mathrm{E}\varepsilon_n \tag{1.7}$$

$$\sigma_\tau = \mathrm{G}\varepsilon_\tau \tag{1.8}$$

Depending of the orientation of the force with respect to the cross-section area, an object can be subjected to normal and shear stress simultaneously due to the same force.

Isotropy is uniformity in all orientations. Glass and metals are examples of isotropic materials [20]. For isotropic materials, the complete characterization of the elastic properties, requires at least two constants, the Young and shear moduli.

In the design of the elastic element, considerations have to take into account the geometry and material of choice. This is done with the aim of keeping the elastic element in the linear section of the stress-strain curve where Hooke's law is still valid.

1.2.1 Examples of elastic elements in force-torque sensors

A comprehensive classification of elastic elements consisting of twelve types of elastic elements, based on their shape, strain gauge positioning and force range has been proposed in [153]. Another way of classification is based on their sensitivity to some specific kind of strain:

- Tension-compression or direct (Fig. 1.4a): A columnar element may be in the form of a solid or hollow cross-section having a circular or square shape. To achieve a four-arm bridge circuit two gauges are aligned parallel to the load axis and two gauges aligned at 90°. The cross-sectional area of the column increases in compression and decreases in tension. This is a typical dual sensing elastic element.
- Bending (Fig. 1.4b): A simple cantilever is an example of a bending load cell. When a force F or a torque M is applied to the free end, it deflects the beam so producing opposite strains at the top and bottom faces. Strain gauges may be installed near the root of the beam to sense tensile and compressive strains.
- Shearing (Fig. 1.4c): Shear elements are based on the fact that shear stresses are proportional to the applied force and are independent of loading position. The shear stresses themselves cannot be measured so pairs of gauges with their grid lines aligned at ± 45° to the neutral axis are installed on both sides of the central portion of the beam to measure principal strains.

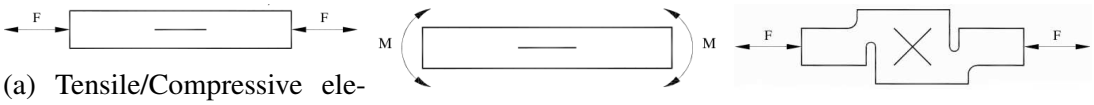

(a) Tensile/Compressive element. (b) Bending element. (c) Shearing element.

Fig. 1.4 Elastic element by sensitivity.

These simple elements can be combined to have sensitivity for forces with arbitrary orientation. The preferred elastic element seems to be variations of the cantilever beams in a cross-beam configuration [97, 139, 109, 143, 135, 145, 4, 64]. Cantilever beam is fixed only on one side. Using them in a cross-beam configuration permits a combination of tensile/compressive and bending elements. Combining multiple elastic elements with this shape has also been explored [98]. They profit from the difference in rigidity between the two elements. With this, they achieved a sensing range from 0.01 N to 1000 N. Some variations of the cross-shaped are shown in Fig.1.8.

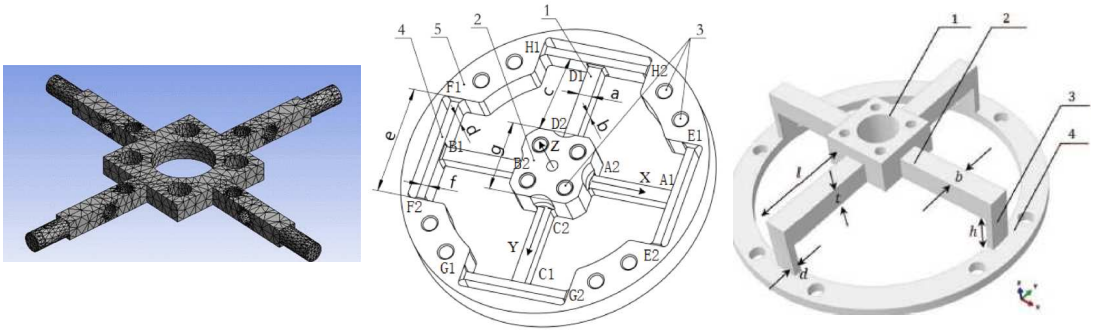

Fig. 1.5 Cross-shaped elastic elements.

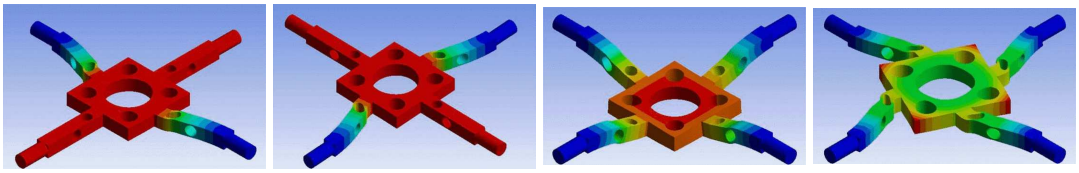

(a) Strain due to x-axis stress. (b) Strain due to y-axis stress. (c) Strain due to z-axis stress. (d) Strain due to shearing stress.

Fig. 1.6 Finite element analysis of choss-shaped elastic element [109].

Another favored shape are cantilever beams in a "Y" configuration [35, 70, 104, 132]. Examples are shown in Fig. 1.7.

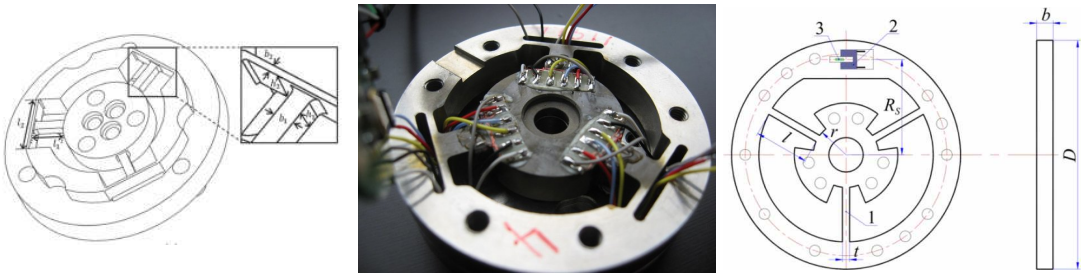

Fig. 1.7 Y-shaped elastic elements.

Besides these two main shapes, other different shapes have been explored in combination with other materials and different sensing technologies. An "E" shape elastic element was used aiming to obtain high measurement sensitivity, overload protection, good linearity, and weak couplings between components [79]. Some 3D-printed S-shaped beams have been used on a capacitive force-torque sensor [76], Fig. 1.8a. Another elastic element used are silicon rubber cubes on a lightweight compliant optical force-torque sensor [2], Fig. 1.8c. Also using silicon rubber, a semi-sphere of rubber has been used coupled with optical technology [128].

(a) 3D-printed structure.

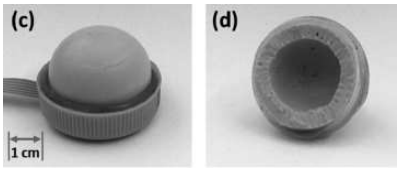

(b) Convex silicon rubber surface [128].

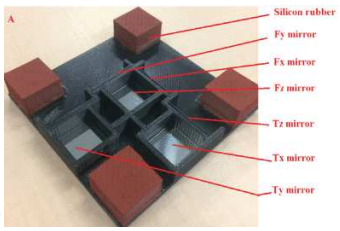

(c) Silicon rubber cubes.

Fig. 1.8 Other elastic element shapes.

Solving a problem of elastic deformations means one should be able to write down all the components of the stress and strain tensors using information on external forces and the elastic moduli. For complex structures, this is usually approximated using finite element analysis, Fig. 1.6.

1.3 Strain Gauges

Several physical effects can be used for measuring strain. Among these effects, there are optical, piezoelectric , and capacitive effects, but by far the most popular is piezoresistive effect [42]. Fundamentally, all strain gauges are designed to convert mechanical motion into an electronic signal. Thus, a strain gauge serves as a transducer that measures a displacement of one section of a deformable component with respect to its other part.

1.3.1 Piezoresistive Strain Gauges

A typical piezoresistive strain gauge is an elastic sensor whose resistance changes with the applied strain (unit deformation), see Fig. 1.9. When a load is applied to the surface, the resulting change in surface length is communicated to the piezoresistive element and the corresponding strain is measured in terms of the electrical resistance, which varies linearly with strain [141]. Since all materials resist deformation, a force must be applied to deform the material. Hence, electrical resistance can be related to the applied force. That relationship is generally called the piezoresistive effect and is expressed through the gauge factor S_ε of the conductor

$$\frac{dR}{R} = S_\varepsilon \varepsilon, \tag{1.9}$$

where R (Ω) is the resistance, dR (Ω) is the change in resistance. For many materials $S_\varepsilon \approx 2$ with the exception of platinum for which $S_\varepsilon \approx 6$. For small variations in resistance not

Material	Gauge factor S_ε	Resistance (Ω)	TCR[1] ($^\circ C^{-1}10^{-6}$)
57 % Cu–43 % Ni	2	100	10.8
Platinum alloys	4.0–6.0	50	2160
Silicon	-100 to +150	200	90000

Table 1.1 Piezoresistive Strain gauges characteristics [42].

exceeding 2% (which is usually the case), the resistance of a metallic wire can be approximated by a linear equation:

$$R = R_o(1 + S_\varepsilon \varepsilon), \tag{1.10}$$

where R_o (Ω) is the resistance with no stress applied. From the materials shown in Table 1.1, S_ε is constant in Ni for a wide range of strain, it can be used under 260 °C. Platinum alloys are used in high-temperature applications. For semiconductive materials, the relationship depends on the doping concentration, it allows for much higher gauge factors.

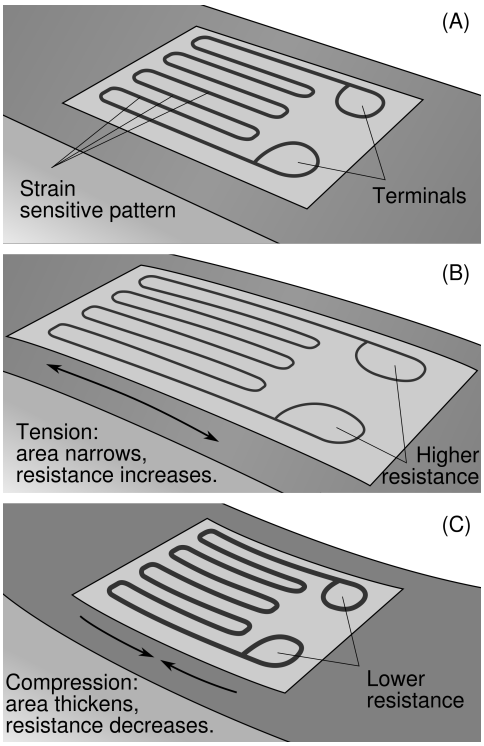

Fig. 1.9 A piezoresistive strain behavior.

The ideal piezoresistive strain gauge would change resistance only due to the deformations of the surface to which the sensor is attached. However, in real applications, temperature,

[1] TCR stands for temperature coefficient of resistance.

material properties, the adhesive that bonds the gauge to the surface, and the stability of the metal all affect the detected resistance. In this context, the term stable refers to the stability of their electron configurations as atoms and as ions. Stable metals do not react with the components of air like oxygen. nitrogen, carbon dioxide, moisture, etc. Because most materials do not have the same properties in all directions, a knowledge of the axial strain alone is insufficient for a complete analysis. Different types of strain require different strain gauge arrangement. When selecting a strain gauge, one must consider not only the strain characteristics of the sensor but also its stability and temperature sensitivity. Unfortunately, the most sensitive strain gauge materials, which are the semiconductors, are also sensitive to temperature variations and tend to change resistance as they age. For tests of short duration, this may not be a serious concern, but for continuous measurement, one must include temperature and drift compensation [99].

Metallic foil Strain Gauge

The metallic foil-type strain gauge consists of a grid of wire filament (a resistor), bonded directly to the strained surface by a thin layer of epoxy resin. Metallic Foil gauges have a low gauge factor. Therefore they require a higher amplification step.
These type strain gauges where the first type of strain gauge technology. It was first developed in 1938 [99], and has been replaced by silicon strain gauge as main force sensing technology in robotics. An image of a typical metallic strain gauge can be seen in Fig. 1.10a.

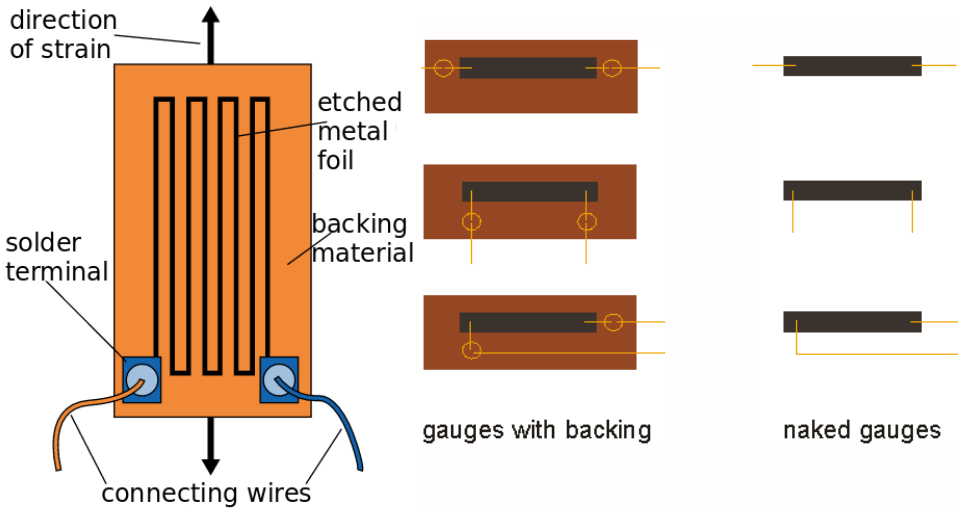

(a) A metallic strain gauge.

(b) A semiconductor strain gauge.

Fig. 1.10 Tactile Sensors.

Semiconductor Strain Gauge

Semiconductor strain gauges are based upon the piezoresistive effects of silicon or germanium. Bonding it to the strained surface needs extra care since only a thin layer of epoxy is used to attach it. The size of a semiconductor strain gauge is much smaller and the cost much lower than for a metallic foil sensor. An example can be appreciated in Fig. 1.10b. While the higher unit resistance and sensitivity of semiconductor sensors are definite advantages, their greater sensitivity to temperature variations and tendency to drift are disadvantages in comparison to metallic foil sensors. This sensing technology is currently the most used.

Wheatstone Bridge

The Wheatstone Bridge is the name given to a combination of four resistances connected to give a null center value. The circuit can be seen in Fig. 1.11. It can be expressed in mathematical terms as:

$$\frac{E_O}{E_I} = \frac{R_1}{R_1 + R_2} - \frac{R_4}{R_3 + R_4} = \frac{R_1 \cdot R_3 - R_2 \cdot R_4}{(R_1 + R_2)(R_3 + R_4)} \tag{1.11}$$

where E_O (V) is the output voltage, E_I (V) is the input voltage and R_i (Ω) is the value of resistance at the i-th position. If $R1 = R_2 = R_3 = R_4$ or $\frac{R_1}{R_2} = \frac{R_3}{R_4}$ then E_O is zero. The resistive elements in the array can have a fixed or variable resistance value.

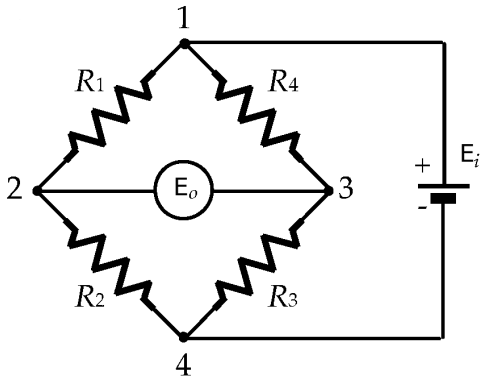

Fig. 1.11 The Wheatstone Bridge circuit.

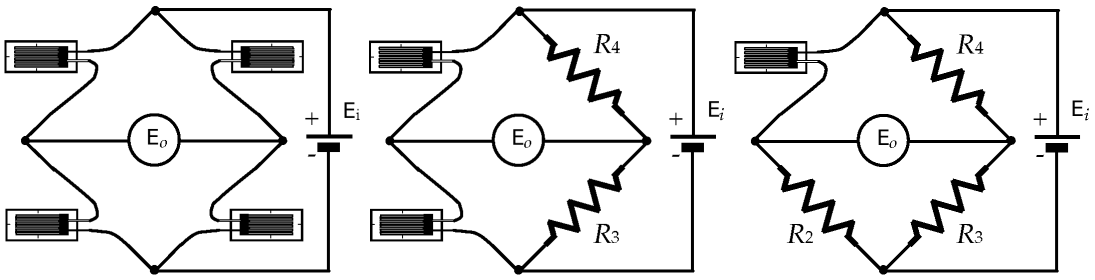

(a) Full Bridge. (b) Half bridge. (c) Quarter bridge.

Fig. 1.12 Types of Wheatstone Bridges.

Depending on the number of variable resistances or strain gauges, it can be classified in a full bridge, half bridge or quarter bridge, see Fig. 1.12. If the variation of resistance ΔR_i is much smaller than the value of R_i, second order factors can be disregarded. This is typically the case for strain gauges.
This arrangement of resistances is well suited for the measurement of small changes in resistance and is, therefore, also suitable for measuring the resistance change in a strain gauge. Another benefit of the Wheatstone Bridge is the fact that it can be arranged to compensate for interference effects, such as temperature, pressure, humidity, magnetic fields, radiation, etc. [57].
The compensation of the temperature expansion is correct only if some conditions are strictly fulfilled. These include:

- symmetry of the bridge,
- identical temperature coefficients of all materials used,
- identical resistances of all parts in the bridge arms which are combined for compensation,
- identical temperatures on all compensating elements in the bridge circuit,
- identical active grid areas.

1.3.2 Capacitive-Pressure Sensors

In simple words, capacitance is the ability of a system to store an electric charge. The capacitive effect can be calculated as:

$$Ca = \frac{q}{E}, \tag{1.12}$$

where q (A) is the current, E (V) is the voltage and Ca (F) is the capacitance . Capacitors are built with two conductive materials with some space in between them. The space can be in vacuum or with some dielectric material. A dielectric material is an electrical insulator that can

be polarized by an applied electric field.

The capacitance is a function only of the geometry of the design (e.g. area of the plates and

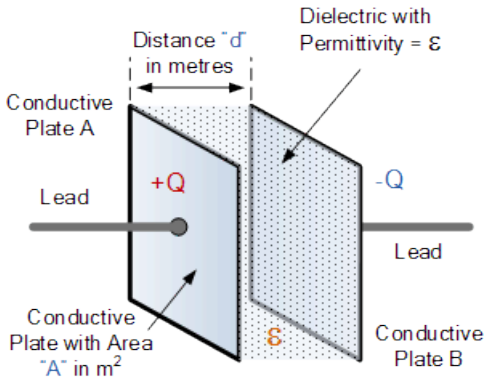

Fig. 1.13 Flat Capacitor.

the distance between them) and the permittivity of the dielectric material between the plates of the capacitor.

A variable capacitance pressure transducer has a capacitive plate (diaphragm) and another capacitive plate (Electrode) fixed to an unpressurized surface gapped a certain distance from the diaphragm, Fig. 1.13. A change in pressure will widen or narrow the gap between the two plates which varies the capacitance. This change in capacitance is then converted into a usable signal for the user [123]. If the shape of the capacitor is flat, the capacitance can be estimated as:

$$Ca = \kappa\varepsilon_0 \frac{A}{d}, \tag{1.13}$$

where κ ($\frac{\mathrm{F}}{\mathrm{m}}$) is the dielectric constant of the material, ε_0 is a constant if the sensor were found in vacuum, A (m^2) is the area of the plates and d (m) is the distance between the plates.

Some dielectrics have a very uniform dielectric constant over a broad frequency range (for instance, polyethylene), while others display strong negative frequency dependence, that is, the dielectric constant decreases with frequency. Temperature dependence is also negative [43].

Examples of force-torque sensors using this technology can be found in [76, 69]. The measuring range is limited to values below 30 N.

1.3.3 Piezoelectric Strain Gauge

The piezoelectric effect is the generation of electric charge by a crystalline material upon subjecting it to stress, or more accurately a redistribution of the electric charge. The charge

generated is proportional to an applied force,

$$Q = \kappa_e F, \tag{1.14}$$

where Q (C) is the charge, κ_e ($\frac{\mathrm{C}}{\mathrm{N}}$)is the piezoelectric coefficient along the orthogonal axes of the crystal cut and F (N) is the applied force.

A piezoelectric strain gauge can convert a changing force into a variable electrical signal, while a steady state force produces no electrical response. Therefore it responds only to changing forces. If the stress is maintained, the charges will be neutralized by the internal leakage. So after some time the piezoelectric material will not send any signal.

Since an applied force can change some properties of the piezoelectric material when the sensor is supplied with an excitation signal, a different property can be exploited for more accurate force sensing.

Certain cuts of a quartz crystal, when used as resonators in electronic oscillators, shift the resonant frequency upon being mechanically loaded. The frequency shift induced by the force is due to nonlinear effects in the crystal. The change of frequency Δfr (Hz) can be described as:

$$\Delta fr = F\frac{Kfr_o^2 n}{l} \tag{1.15}$$

where F (N) is the applied force, K is a constant, fr_o (Hz) fundamental frequency when unloaded, n is the number of the overtone mode (it allows to use the quartz in a frequency higher than fr_o and l (m) is the size of the crystal [42]. An image of this kind of sensor can be seen in Fig. 1.14.

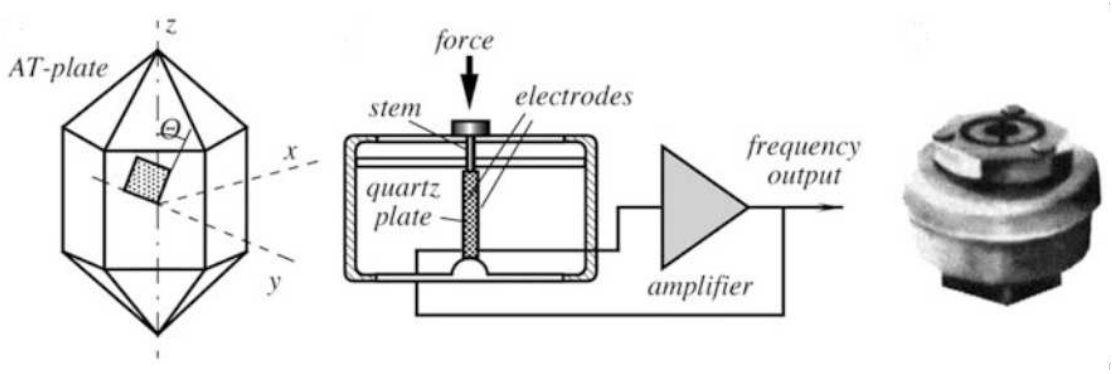

Fig. 1.14 A piezoelectric strain gauge [42].

A fundamental problem in all force sensors that use crystal resonators is based on two contradictory demands. On one hand, the resonator shall have the highest possible quality factor which means the sensor has to be decoupled from the environment and possibly should

operate in vacuum. On the other hand, application of force or pressure requires a relatively rigid structure and substantial loading effect on the oscillation crystal, thus reducing its quality factor.

1.3.4 Optical Force Sensor

Although not considered strictly strain sensors, they work by a similar principle of measuring the deformation or displacement of a body. An optical force sensor is typically composed of a light source, a photosensor, a solid object modifying amount of light incident on the optical detector are necessary to measure displacement between an unmovable and a flexible part of the optical sensor.
The photosensors have drawbacks such as nonlinearity and temperature sensitivity, however, they are considerably reliable, cheap and allow simplifying the construction of the design. A displacement can be detected by interrupting light between source and detector, changing the intensity of reflected light or relative movement of source and detector [56]. In this cases the relationship with the strain is completely dependent on the geometry of the sensor. Lately some

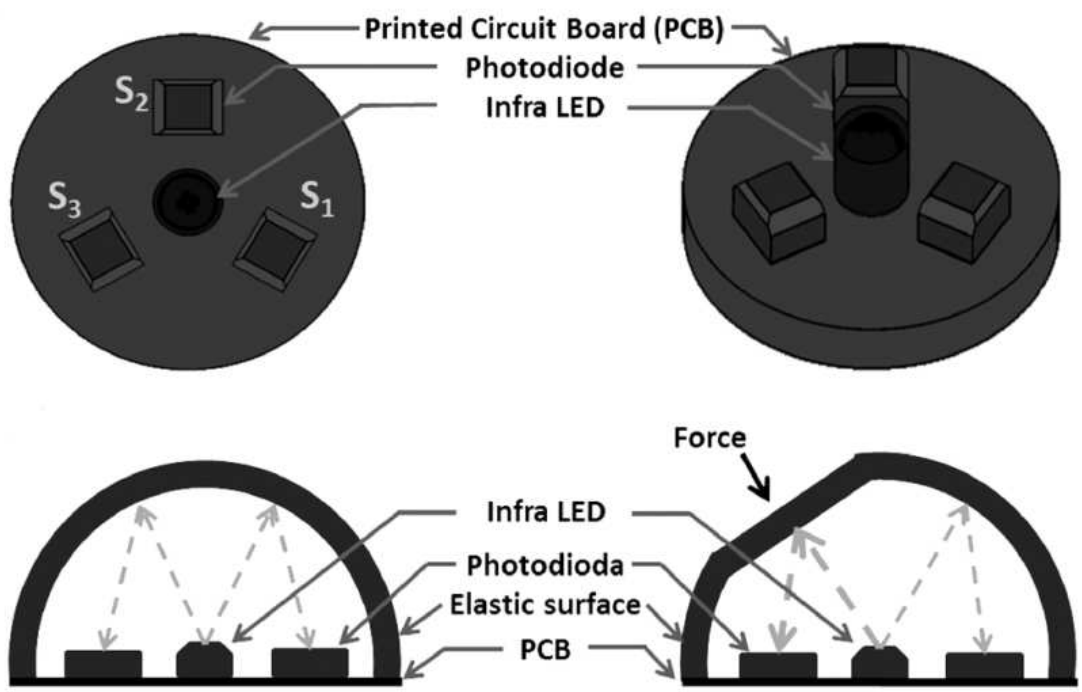

Fig. 1.15 An optic force-torque sensor [128].

force-torque sensors based in optical technology have been developed. Their aim is to have an easy manufacturing process, durability, scalability, low cost and having good sensitivity [128].

A drawback is that the behavior is nonlinear which complicates the calibration procedure. They have yet to become widely used in applications of 100 N or more.

Fiber Optic Sensor

Fiber optic sensors offer a promising alternative to electric measurement systems. For the fiber optic sensor the optical detector is embedded into a holder that acts as a resilient component (spring). Fiber optic FT sensors have recently been presented with varying degrees of freedom (DoF). Fiber optic sensing principles can be categorized by the physical value being measured. Among others the most frequently used measured variables are intensity and wavelength.

Light is reflected back into the fiber by a mirror connected to a deformable structure. The intensity of reflected light depends on the axial and angular deformation of the structure. The reflected intensity is measured and interpreted as axial force. Bend losses in the fiber cannot be distinguished from intensity variation by the measuring device. Measuring the wavelength instead of intensity offers the possibility to become almost independent of losses in the optical fiber. Aside from certain material constants and design parameters the reflected wavelength is determined by mechanical and thermal conditions as given by

$$\frac{\Delta\lambda}{\lambda_0} = (1-p_{eff})e + \left[(1-p_{eff})\alpha + \frac{1}{n_0}\frac{dn}{dT}\right]\Delta T, \tag{1.16}$$

with nominal wavelength λ_0 (m), photoelastic coefficient of the fiber $peff$ (Pa^{-1}), thermo-optic coefficient $\frac{dn}{dT}$ (K^{-1}), effective refractive index n_0, linear strain in direction of the fiber axis e, and temperature change ΔT (K).This type of force sensing technology ranges up to 20 N [53].

1.4 Tactile Sensor Technologies

In general, the tactile sensors belong to the special class of force or pressure transducers that are characterized by small thicknesses.
Tactile sensors sensing technologies, similarly to force sensors, can be: capacitive, piezoresistive, piezoelectric, magnetic and optical.

- Piezoresistive sensors (e.g. [61, 124, 68]) are made of materials whose resistance changes with the applied force and can therefore vary the voltage of the signal.
- Capacitive sensors (e.g. [138, 85]) rely on their change in capacitance value as the dielectric between the two conductive plates is compressed. The capacitance value variation can be interpreted by the control circuit.

- There are piezoelectric sensors (e.g. [118]) that create a voltage signal as they are deformed due to their piezoelectric properties.

There are more types of tactile sensors (optical, magnetic etc.), but the mentioned ones are the most commonly used in the industry [47, 46, 150].

(a) Resistive 3D shaped tactile sensor [73].

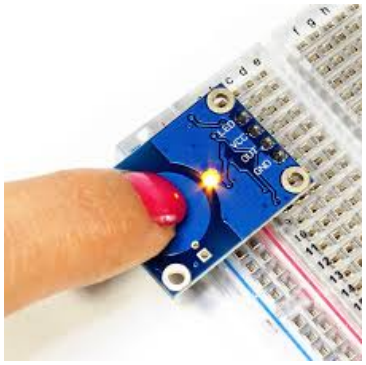

(b) A capacitive touch sensor.

(c) A capacitive slip tactile sensor.

Fig. 1.16 Tactile Sensors.

The tactile sensors loosely can be subdivided into several subgroups [41].

- Touch sensors detect and/or measure contact forces at defined points. They are binary, namely—touch or no touch. It can be analog and use a force measure for having a trigger threshold behavior.
- Contact Sensors detect physical coupling between two objects, regardless of forces. An example is a capacitive touchscreen on a touch-sensitive monitor (e.g., smartphone).
- Spatial Sensors detect and measure the spatial distribution of forces perpendicular to a predetermined sensorized area. A spatial-sensing array can be considered to be a coordinated group of touch sensors.
- Slip Sensors detect and measure the movement of an object relative to the sensor. This can be achieved either by a specially designed slip sensor or by the interpretation of the data from a touch sensor, contact sensor, or a spatial array.

Since their aim is not to measure forces, typically they are not very accurate when using it for force-torque sensing.

1.4.1 Tactile sensor arrays

Tactile sensor arrays, also known as artificial skins, are used in many fields of engineering including neuroprosthetics, humanoid robotics, and wearable robotics [82]. They can be classified as spatial tactile sensors. As implied by the name, they are arrays of tactile sensors arranged, typically, in a distributed manner over a surface. This forms a discrete area where tactile sense is possible. The area is not fully cover and contains gaps between the individual tactile sensors. In humanoid robotics, the artificial skins are usually mounted on the surface of robots in order to detect physical interactions with the external world. They are mainly used to detect contacts. Some attempts have been done to use them as force sensors [66].

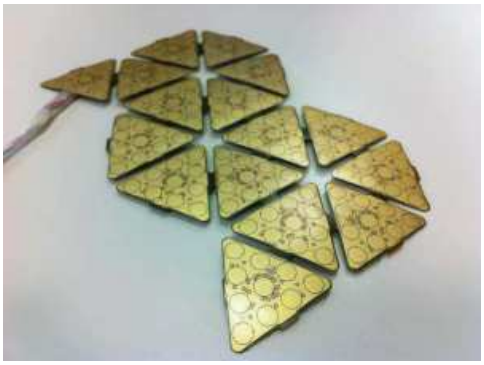

Fig. 1.17 A tactile sensor array.

1.5 Force Sensors

Even if there are many possible sensing technologies, the actual sensors used in the robots, regarding force-torque sensing, can be mainly divided into three categories:

- single-axis force sensor
- single-axis torque sensor
- multi-axis force-torque sensor

In robotics, single-axis torque sensors are typically installed at the joints. Joint torque information is crucial because it is directly related to the motor actuating the joint, making them essential feedback for force-torque controllers. Since joint torque sensors provide this information directly, they are commonly used.

Single-axis force sensors are only able to give information about one axis. Multi-axis force-torque sensors can easily give the same information and more.

Six axis FT sensors have an arrangement of strain gauges designed to measure the forces and torques sensed at the sensor frame. Six axis FT sensors give complete information about the sum of the forces and torques exchanged between two bodies. As a result, six axis force-torque sensors are able to directly convey information about interactions with the environment.

Although many robots have six axis FT sensors, they are not exploited to their full potential [32]. Since the six axis FT sensors have the most wasted potential, they are the main focus of the thesis.

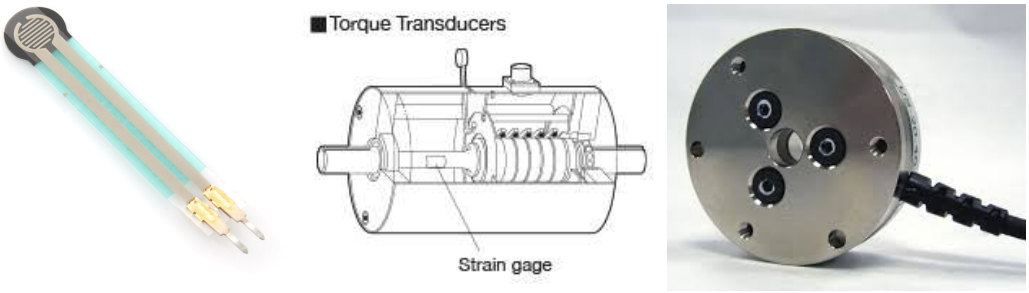

(a) A single-axis force sensor. (b) A single-axis torque sensor. (c) A six axis FT sensor.

Fig. 1.18 Force-torque Sensors.

1.5.1 Commercially Available Six Axis Force-torque Sensors

Looking at the main options in the market may allow to know the most used technology. This way the impact of this research will be more widespread by focusing on that technology. Six axis FT sensors are sold in a big variety of sizes and ranges. Its application span from medical instruments to big industrial manipulators, this includes wearable robotics and other types of robots.

What follows is a non-exhaustive comparison of commercial six axis FT sensors for robotics. The comparison is summarized in Table 1.2. Even if the oldest technology is the metallic foil strain gauge, only one company clearly states they use this technology. Among the sensors in the comparison, most of them use the silicon strain gauge technology. Some companies offer custom calibration upon request. Some specify the possibility to offer a Complex Loading Calibration. By sacrificing some resolution the range of the sensor is guaranteed even under loads that combine different axis.

Most of them recognize the issue of temperature drift as stated in the data sheets of the reviewed sensors. Nonetheless, just a minority offer temperature compensation and in some cases only upon explicit request.

It is important to point out that the information offered in the data sheets of the sensors is not

standardized. Information such as bandwidth, non-linearity, type of sensing technology and expected accuracy is not available for all sensors' data sheets. Some sellers, offer different calibrations for the same sensor. In those cases, only the calibration with the higher range is displayed. The lack of standardized information prevents having a more in depth analysis of the commercial solutions. The shape of the elastic element is not available in any of the data sheets.

It is worth noticing that the Axia80, from ATI, offers dynamically changing calibration. It goes from a high calibration range to a lower calibration range. Is interesting since usually the accuracy is given as a percentage of the full scale. Therefore reducing the full scale reduces the error in the measurements. From all sensors reviewed, it is the only one with this feature.

The range of six axis FT sensors in the comparison is limited to sensors that have a range from 120 N to 1000 N for the forces and 3 Nm to 60 Nm for the torques. This range was considering the requirements of a the 33 kg robot as middle point. The range for a 33 kg robot is 500 N for the forces and 30 Nm for the torques.

Silicon strain gauges are the most common. This type of sensor is based on the piezoresistive technology using semiconductors as material. For this kind of material, the model of the resistance can be approximated to a linear model. As a result, a linear model is also the main approach for the calibration model. Even if they are sensitive to temperature as well.

Sensor	Company	Technology	Fx, Fy (N)	Fz (N)	Tx,Ty (Nm)	Tz(Nm)	Dimension (mm)	Accuracy	Nonlinearity
AD2.5D	AMTI	Strain Gauges Transducers	2224	4448	112	56	63,5*63,5	N/A	± 0.2% Full Scale
FS6	AMTI	Strain Gauges Transducers	±1100	±2200	±56	±28	63,4*37,8	N/A	± 0.2% Full Scale
mini45	ATI	Silicium strain gauges	±580	±1160	±20	±20	15,7*45	0.1% to 5% due to temperature	N/A
mini58	ATI	Silicium strain gauges	±1400	±3400	±60	±60	30*58	0.1% to 5% due to temperature	N/A
75E20A4	JR3	Foil strain gauges	±1000	±2000	±200	±200	50,8*191	±0,25%	N/A
FTS-Theta	Shunk	Silicium strain gauges	±2500	±6250	±400	±400	61,1*155	±1%	N/A
3713A	SunriseInstruments	Strain Gauges Transducers	±400	±800	±14	±14	25*135	N/A	N/A
HEX-H	OPTOFORCE	Optically Measured deformation	±200	±200	±15	±10	43.5*70	Can measure shear forces. More durability	<2%
Barrett	Barret Technology	Silicium strain gauges	±80	±135	±2.75	±2.75	12*90	N/A	N/A
30E12A4	JR3	Foil strain gauges	±200	±400	±16	±16	19*45	N/A	0.50%
FT300	Robotiq	Capacitive	±300	±300	±30	±30	37,5*75	1N,0.02Nm	N/A
FTC050	Shunk	opto-electric measurement	±450	±400	±7	±15	48,5*161	N/A	N/A
FT nano 25	Shunk	Silicon Strain gauges	±250	±1000	±6	±6	21,6*25	N/A	N/A
kms40	Weiss Robotics	Not mentioned	±120	±120	±3	±3	27*76	N/A	N/A
Axia80	ATI	Silicon Strain Gauges dual calibration	±500 ±200	±900 ±360	±20 ±8	±20 ±8	25.4*104	<2%	N/A

Table 1.2 Commercially available six axis FT sensors.

1.6 Conclusion

The principles in which the force-torque sensing is based have been discussed as well as the components of a force-torque sensor. In robotics, most force-torque sensors are based on the relationship between elastic deformation and forces. The knowledge of principles in which they are based, help anticipate some of the behaviors that can be expected from the sensors. The fact that the silicon strain gauge is the main technology used in force-torque sensors coupled with the knowledge that this technology is sensitive to temperature helps to anticipate the possibility of temperature drift. The complexity of the arrangement of strain gauges in the elastic element increases with the number of axes that are meant to be measured. This makes it hard to fulfill all the requirements to perform temperature compensation at hardware level. Understanding the principles behind tactile sensors allows having bases to believe they can be used as force-torque sensors.

While knowledge of the principles gives a clear picture of what happens inside the sensor, the way the sensors are actually used may help understand what should be expected from these sensors. The way force-torque sensing is used in Robotics is discussed in Chapter 2.

Chapter 2

Use of force-torque sensing in Robotics

The principles in which force-torque sensing is based are important to understand the inner workings of force-torque sensors. Having a clear picture of how they are used allows to understand what is expected of these sensors. Among other things, the information of force-torque sensing could be possibly used for controlling dynamic motions or ensure safety when interacting with other bodies, especially humans. In other words, this information allows knowledge of the contacts arising from interactions with the environment or other bodies and could permit their capitalization. Providing force information to the robots is known to increase their operational ability [116]. In this chapter, the main locations of force-torque sensors in robotics are described. Some of the uses of these sensors are briefly mentioned. The dynamic equations of motion are detailed to showcase the connection between force-torque sensing and dynamic motions. The state of the art for estimation of force-torque sensing quantities such as the contact forces and joint torques are provided. Lastly, the current state of dynamic motions performed by robots is mentioned.

2.1 Location of Force-Torque sensors on Robots

Robots with their base fixed to the ground are called fixed based robots. Manipulators fall in this category. When the base of the robot is not fixed to the ground it is called floating base. Single axis torque sensors are position at the joints due to their direct connection with the actuation torque. This makes them a typical force-torque sensor present in robots [122, 147, 83]. On the other hand, six axis force-torque (FT) sensors have been considered important in the design of floating base robots, such as humanoids [104, 55, 9, 62, 63, 34]. Six axis FT sensors have mainly two types of locations in robotics. Either at the end-effector position (wrists and feet), see Fig. 2.1, or near the base of the robot, Fig. 2.2.

FT sensors in the end-effector position are the most widely used. Being less affected by dynamic effects and gravity they have less dynamic errors in the measurements [48]. Although the position can be classified as end-effector, wrists and feet positioned FT sensors have different expected uses. The wrist positioned sensors are mostly used for manipulation tasks while the feet are meant to measure ground reaction forces. Manipulation tasks are mainly described as slow and short motions. Contrary to wrist positioned sensors, the sensors at the feet could experience fast or slow motions depending on the task. This has an impact in the expected excitation of the sensors and the relevance of dynamic effects on the sensor.
FT sensors at the base position are useful to detect contacts along the kinematic chain [121, 48]. As such, they are able to detect unexpected collisions which might happen in both slow or fast motions. In floating base robots the base is typically the torso or the pelvis. Therefore, FT sensors in the shoulders or the hip are classified as near the base.
Regardless of their position this sensors are likewise affected by any extra weight and inertia of a load at the end-effector [48]. By the nature of what they measure and considering their typical locations in robots, six axis FT sensors and single axis torque sensors can provide direct information about forces at contacts and torques at the joints respectively.
Installing force sensors on the robots can result in high maintenance prices, high noise values, soft structure, and complication of the system's dynamic equations. It is well known that information of a force sensor has much noise. Furthermore, an unstable state can be caused by the narrow bandwidth of force information by a force sensor. [67].

(a) Sensor at the wrist of a fixed base robot.

(b) Sensor at the foot of a legged robot.

Fig. 2.1 Examples of force-torque sensors placed near end-effector positions.

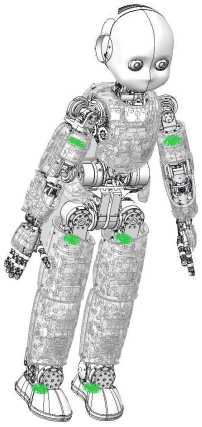

(a) Sensor at the shoulder and hips of floating humanoid.

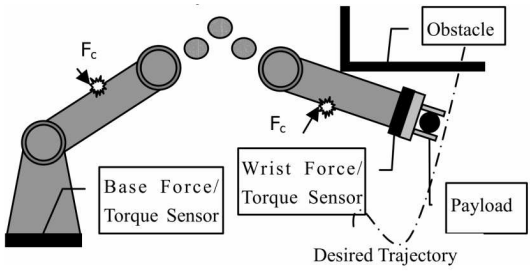

(b) Sensor at the base and wrist on fixed based robot.

Fig. 2.2 Examples of force-torque sensors placed near the base positions.

2.2 Force-Torque sensor uses in robotics

Six axis force-torque (FT) sensors have been used in robotics systems since the 1970's [140]. They have been widely used in fixed based robots, mainly for fine motions [48]. The use of the FT sensor information can be broadly classified into two depending if the information is used directly or not.

Direct use of the information implies that the force or torque knowledge is used to generate some response or take a decision. The simplest use of a force-torque sensor is as a threshold for contact detection. By using a threshold on the forces on the z-axis, the foot in contact with the ground is identified [107, 32]. This can be generalized to logic branching behaviors based on thresholds on the value of the forces [48]. This includes the detection of collisions [51] or slippage conditions [90].

Another way to use directly the information is by using it as feedback for control applications. Joint torque sensors have been successfully used in control applications in the past [74]. It has been shown that joint torque feedback is a fundamental part of force, compliance and impedance control [1, 80, 136]. Conceptually, introducing joint torque sensor feedback in the control loop is similar to introducing a six axis FT sensor feedback [48]. After a contact is established it can be desirable to control the actual interaction between objects. A survey on different interaction control schemes has been presented [22]. These schemes where proposed and tested in fixed based robots. The need for the full dynamic model and force-torque sensing is clearly stated. A six axis FT sensor near the end effector was used. This sensor can also be used in control applications with multiple contact scenarios [59]. In some robots, the

local stability is enforced by a proprietary stabilizer, which exploits the IMU and force-torque sensor feedback [72]. Some whole-body controllers able to exploit contact information have been developed in the past [119]. They require to sense the reaction forces at the contacts to overcome effects of unmodeled friction at the joints due to the the gearing mechanisms.
The indirect use of the information implies that the information provided is processed to generate other knowledge that is then used. Given the relationship between force, mass and acceleration, force information can be used to estimate quantities related to mass and acceleration. For this reason, FT sensors have been used to estimate inertial parameters in fixed based robots [144, 108, 49, 101]. Measurements from six axis FT sensors have also been exploited to track the center of mass(CoM), center of pressure (CoP) and zero moment point(ZMP) [111]. These quantities are commonly used in whole body controllers. They can be used as part of the information required to estimate the momentum of robots [113]. Given the elastic nature of the principles involved in FT sensors the information they provide have been also been used to estimate micro-displacements [48]. Another indirect use of the information is the exploration and shape reconstruction of objects [15].
Given the possible uses of FT sensing information, especially its use as feedback information, FT sensors have permeated through many robotic research areas such as physical human-robot interaction, exoskeletons, teleoperation, haptics, surgical robots, industrial robots, force control and locomotion to name a few [122].

2.3 Robot Dynamics and force-torque sensing quantities

A robot can be seen as a combination of multiple bodies acting as a whole (a multi-body system). An element q can be defined as the following triplet: $q = \left({}^{A}p_B, {}^{A}R_B, s\right)$ where ${}^{A}p_B \in \mathbb{R}^3$ denotes the position of the base frame with respect to the inertial frame, ${}^{A}R_B \in \mathbb{R}^{3\times3}$ is a rotation matrix representing the orientation of the base frame, and $s \in \mathbb{R}^n$ is the joint configuration characterising the shape of the robot. The velocity of the multi-body system can be characterized as the triplet $\nu = \left({}^{A}\dot{p}_B, {}^{A}\omega_B, \dot{s}\right) = (\mathrm{v}_B, \dot{s})$, where ${}^{A}\omega_B$ is the angular velocity of the base frame expressed w.r.t. the inertial frame, i.e. ${}^{A}\dot{R}_B = S\left({}^{A}\omega_B\right){}^{A}R_B$. A more detailed description of the floating base model is provided in [131]. Applying the Euler-Poincaré formalism [88] to the multi-body system, yields the following equations of motion for a robot with n_c distinct contacts with the environment:

$$M(q)\dot{\nu} + C(q,\nu)\nu + G(q) = \mathbb{B}\tau + \sum_{k=1}^{n_c} J_{C_k}^T \mathrm{f}_k \tag{2.1}$$

where $M \in \mathbb{R}^{(n+6)\times(n+6)}$ is the mass matrix, $C \in \mathbb{R}^{(n+6)\times(n+6)}$ accounts for Coriolis and centrifugal effects, $G \in \mathbb{R}^{n+6}$ is the gravity term, $\mathbb{B} = (0_{n\times 6}, 1_n)^T$ is a selector matrix, $\tau \in \mathbb{R}^n$ is a vector representing the actuation joint torques, and $f_k \in \mathbb{R}^6$ denotes the force applied by the environment on the robot at the k-th contact, also called contact forces or external force-torques. The Jacobian $J_{C_k} = J_{C_k}(q)$ is the map between the robot's velocity v and the linear and angular velocity at the k-th contact link. From eq. (2.1), it can be seen that force torque related quantities involved directly with the motion of a robot are the joint torques and the contact forces, Fig. 2.3. Contact forces have great relevance in stabilizing the robot because it is through these forces that the robot can actuate the underactuated degrees of freedom (DoF), like the center of mass (CoM) position and the floating base orientation [23]. Using contact force information is also possible to improve grasping task such as opening doors or turning valves [77]. Likewise, the relevance of joint torques is derived from its relation with the output of the motors. Therefore information of these quantities is crucial for controlling the dynamic motions of a robot. Since there is a direct relationship between force and acceleration, the more dynamic the motions more important it is to have accurate force sensing.

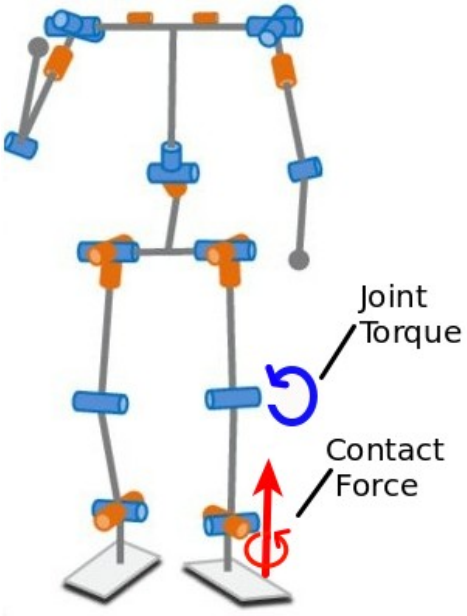

Fig. 2.3 Joint torque and contact force in a robot.

Depending on the available information, it is possible to use eq. (2.1) to estimate the joint torques, the contact forces or both. What follows is a small review of the state of the art on contact force and joint torque estimation. Using end-effector FT sensors for contact force and joint torque sensors for joint torque values are not included in the review since they measure

these quantities. This means there is no estimation. Some of the approaches are able to estimate both type of quantities. The different solutions presented use different combinations of the following sensors: tactile sensors, near base six axis FT sensors, inertial measuring units (IMU), encoders, current sensors, cameras, and joint torque sensors.

2.3.1 Contact Force Estimation

Many approaches have been developed to estimate contact forces. They typically separate this problem in three phases: contact detection, contact location estimation, and contact force estimation. This corresponds to the first three stages of the collision event pipeline [51].
A natural solution for the first two phases of the contact force estimation is the use of distributed tactile sensing. Some attempts have been done to calibrate these sensors to obtain also the force at the contact [23, 28, 68]. In these cases, FT sensor information was used to calibrate the tactile arrays. Therefore the accuracy of the calibrated skin will at best be as good as the accuracy of the sensor used to calibrate it. These solutions are able to estimate multiple contacts.

There have been many solutions to contact force estimation based on the momentum-based residual signal concept [81]. The residual is calculated as the difference between the generalized momentum of the robot and the expected generalized momentum due to the commanded torque. This concept sets threshold values for the residual signal. When the value is exceeded it is considered that a contact is detected. The direction of the contact is also reconstructed using the robot generalized momentum. The residual signal grows exponentially with a contact and the actual magnitude of the contact force is not provided. The original residual solution solves the first two phases of contact detection and localization of the link in which the contact happens. Different extensions of the residual have been extended to obtain the value of the contact force. Using external sensors like a Kinect [84] or relaying heavily on the robot model coupled with a particle filter [87]. The original residual approach assumes the robot is able to reach a commanded torque value. Some other solutions have been proposed to circumvent this limitation and still use the residual concept. Others have exploited current sensors and known quasi-static robot configuration to estimate the joint torques in the unloaded case and through comparison with the loaded case reconstruct the forces [89]. An extension of the residual method estimates the joint torques with current measurements taking into consideration backlash and friction [40]. Although the joint torques are estimated, their value are only used as threshold to detect contacts. A non-linear model based on binary-tree prediction has been used when the model of the motor is not trusted using discrepancies in the commanded position [17, 18]. In the last mentioned solution the magnitude of force was not reconstructed. The residual method has some limitations such as the need for enough DoF

for a full contact reconstruction (three forces and three torques) and the inability of detecting contacts in the nullspace of the Jacobian. This information is not lost when using six axis FT sensors. Even so, they are theoretically able to distinguish multiple contacts in the same kinematic chain which six axis FT can not do alone.

A strategy to estimate contact wrenches given whole-body distributed FT and tactile sensors was proposed in [30] and extended in [129, 29]. The estimation strategy relies on the joint torque estimations described by [44]. As a by-product of the rearranged Newton-Euler recursion, authors present an algorithm to compute the total (external) contact force acting on a subpart. Subparts are defined by the kinematic subchains obtained by dividing the robot at the level of the available FT sensors. An exact estimation can be given only if there is one contact wrench per subchain. Otherwise, a linear least-squares is proposed to obtain an approximated solution. The contact force is estimated at any subchain even if the contact is far from the FT sensor. Therefore is not strictly measured. This relies heavily in the accuracy of the FT sensors and is susceptible to errors in the model, encoders and IMU measurements used to propagate gravity values. Similarly, the orientation and the velocity of the floating base have been used in a state estimator able to rebuild, in a single state vector, floating base kinematics, contact forces, and external contacts. The state estimator is based on extended Kalman filtering [13]. No force-torque data is used, but the possibility to improve the performance of the estimator with this data is clearly mentioned.

A method for estimating the contact forces using a body-suit of motion capture system was proposed in [105]. A recursive neural network is used to learn the forces based on physics-based optimization. Even if the estimation depends on centroidal dynamics, the collected data set is collected through human motions and are not likely to be equally performed by floating base robots. Contact detection is still required.

A way to make the estimation of localization of contact more robust has been to perform sensor fusion through the combination of hypothesis using a likelihood probabilistic estimation [38]. Each sensor involved and the model provide a different hypothesis with its respective likelihood in a discretized 3D cartesian space. Multiple contacts can be detected, but no value of the force is provided. Another way to fuse data is through the use of the extended kalman filter [33]. In this case, a restriction to the use of flat tactile array prevents from estimating other contact forces beside the one at the foot.

In general, these solutions can be grouped in using tactile sensing as a substitute, using joint torque information, propagating FT sensor measurements using the model or fusing multiple type of sensors. Even among these there is no solution that can detect multiple contacts in every situation in a fast for the possible range of forces.

2.3.2 Joint Torque Estimation

There are many robots that do not include joint torque sensors [91, 17, 89]. Adding series Elastic Actuators (SEA) [103] is a common solution to estimate joint torques. Often, this solution adds a degree of compliance into the robot, which makes the control and planning tasks more complex. Based on the same elastic principle, joint torque estimation can also be achieved by measuring the deformation in the Harmonic Drive to estimate Joint torques [152]. Using any of these techniques for joint torque estimation requires mechanical changes, which may sometimes be not feasible. Another possible solution is to use current measurements and the motor model to estimate the motor torque. The whole model with the gearbox should be taken into account to provide the joint torque [149].

There are techniques that combine the distributed FT to estimate joint torques [44, 29, 30, 129]. The resulting accuracy of the joint torque value depends on the performance of the FT sensor. Some extensions of the momentum-based residual signal method have required to provide some estimate of the joint torques [40, 89, 17, 18]. Even if control actions have been successfully executed with these estimations, accuracy comparisons are not provided.

2.4 A multi-body estimation scheme for contact forces and joint torques

What follows is a description of the theoretical framework proposed in [44, 30] for the estimation of contact force and joint torques on chains, later extended for the whole-body case in [129]. The algorithm consists in cutting the floating-base tree at the level of the (embedded) FT sensors obtaining multiple sub-trees that we call sub-models. The base of a sub-model is the link in the sub-model connected to the FT sensor closer to the floating-base. Each sub-model is considered an independent articulated floating-base structure governed by the Newton-Euler dynamic equations [129]. In the example in Fig. 2.4, measured force-torques are indicated in green and are pointing towards the floating-base, while unknown contact force-torques are drawn in red. There are $n = 5$ FT sensor in the system, that is then decomposed in $n+1 = 6$ sub-models. Other contact force-torques (red arrows in Fig. 2.4 and Fig. 2.5) are estimated with the procedure described below.
This algorithm is used as an evaluation tool in Chapter 4, to calculate the reference wrenches in Chapter 5 and extended in Chapter 7 to consider information from the artificial skin.

2.4.1 Notation

Notation used through the thesis

A,B	Coordinate frames.
$\|\cdot\|$	Euclidean norm.
A	Inertial frame.
${}^{A}R_{B} \in \mathbb{R}^{3\times3}$	3D rotation matrix from B to A
${}^{A}o_{B} \in \mathbb{R}^{3}$	Coordinates of the origin of frame B expressed in frame A.
$u, v \in \mathbb{R}^3, u^\wedge \in \mathbb{R}^{3\times3}$	Skew-symmetric matrix-valued operator associated with the cross product in $\mathbb{R}^3$, such that $u^\wedge v = u \times v$.
${}^{A}\omega_{A,B}$	with ${}^{A}\omega^{\wedge}_{A,B} = {}^{A}\dot{R}_{B}\,{}^{A}R_{B}^{\top}$ Angular velocity of frame B with respect to the frame A expressed in frame A.
${}_{B}\mathrm{f} = \begin{bmatrix} {}_{B}f \\ {}_{B}\tau \end{bmatrix}$	Coordinates of the 6D force f expressed in the B frame.
${}_{A}X^{B} = \begin{bmatrix} {}^{A}R_{B} & 0_{3\times3} \\ {}^{A}o_{B}^{\wedge}\,{}^{A}R_{B} & {}^{A}R_{B} \end{bmatrix}$	6D force transformation from B to A.
$\langle s, p \rangle$	Dot product between vectors s and p.

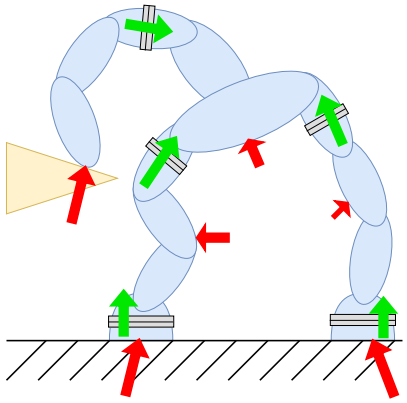

Fig. 2.4 A multi-body system with internal six-axis FT sensors.

2.4.2 Contact Force Estimation

In the simple case of one body, we define the *sensor proper* acceleration of body B of the frame B w.r.t. to the frame A as ${}^{B}\alpha^{g}_{A,B} = \begin{bmatrix} {}^{B}R_{A}({}^{A}\ddot{o}_{B} - g) \\ {}^{B}\dot{\omega}_{A,B} \end{bmatrix}$, where ${}^{A}g$ is the gravitational acceleration in the inertial frame [129].

We also define the inertia tensor of body B expressed with respect to frame B as ${}_{B}\mathbb{M}_{B} = \begin{bmatrix} m1_{3\times3} & m\,{}^{B}c^{\wedge} \\ -m\,{}^{B}c^{\wedge} & {}_{B}\mathbb{I}_{B} \end{bmatrix}$, where m is the body mass, ${}^{B}c$ are the coordinates of the center of mass in frame B and ${}_{B}\mathbb{I}_{B}$ is the 3D inertia matrix of the rigid body, expressed with the orientation of frame B and with respect to the frame B origin.

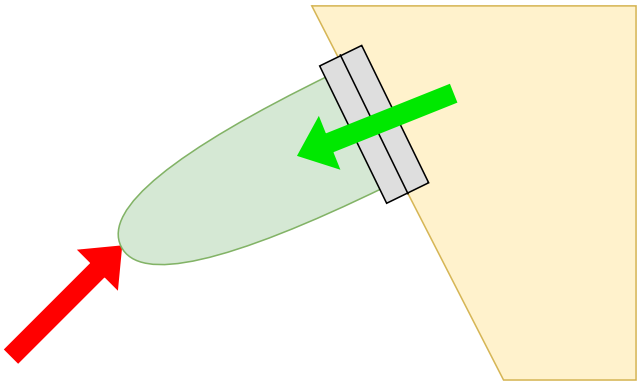

Fig. 2.5 Graphical representation of equation (2.2).

Using the *sensor proper* acceleration of body B ($^{B}\alpha^{g}_{A,B}$) , the angular velocity of the link B in the B frame ($^{B}\omega_{A,B}$), FT sensor measurements ($_{B}\mathrm{f}^{s}$) at a given instant and the inertia tensor of body B ($_{B}\mathbb{M}_{B}$), we can estimate the contact force-torque $_{B}\mathrm{f}^{x}$ by writing the Newton-Euler equations for body B:

$$_{B}\mathrm{f}^{x} = {}_{B}\mathbb{M}_{B}\,{}^{B}\alpha^{g}_{A,B} + \begin{bmatrix} {}^{B}\omega^{\wedge}_{A,B} & 0_{3\times3} \\ 0_{3\times3} & {}^{B}\omega^{\wedge}_{A,B} \end{bmatrix} {}_{B}\mathbb{M}_{B} \begin{bmatrix} 0_{3\times1} \\ {}^{B}\omega_{A,B} \end{bmatrix} - {}_{B}\mathrm{f}^{s}. \tag{2.2}$$

In (2.2) the term $_{B}\mathrm{f}^{s}$ is the only one that does not depends on acceleration, velocity and the inertial parameters of the body. For convenience, we will indicate all other terms as:

$$\begin{aligned} {}_{B}\phi_{B}({}^{B}\alpha^{g}_{A,B}, {}^{B}\omega_{A,B}) = {}_{B}\mathbb{M}_{B}\,{}^{B}\alpha^{g}_{A,B} \\ + \begin{bmatrix} {}^{B}\omega^{\wedge}_{A,B} & 0_{3\times3} \\ 0_{3\times3} & {}^{B}\omega^{\wedge}_{A,B} \end{bmatrix} {}_{B}\mathbb{M}_{B} \begin{bmatrix} 0_{3\times1} \\ {}^{B}\omega_{A,B} \end{bmatrix}. \end{aligned} \tag{2.3}$$

From here on, we will omit the dependency on the *proper sensor acceleration* and on the *body angular velocity* indicating this term as $_{B}\phi_{B}$ and call it *net force-torque* acting on the body B even if this term does not include the force-torque due to gravity.

A *multi-body* system is composed of two sets. A set $\mathfrak{L}$ of n_L rigid bodies (*links*) interconnected by n_J mechanisms (*joints*) constraining the relative motion of a pair of links. $\mathfrak{J}$ is the set of joints, represented as the two links interconnected by the joint. Each body B is associated with a frame B rigidly attached to it.

When considering the case of a multi-body system, for each link in a sub-model $L \in \mathfrak{L}_{sm}$ we indicate with $\beth_{sm}(L)$ the set of links that are connected with L in the floating-base tree, but

belong to a different sub-model., i.e.:

$$\beth_{sm}(L) := \{D \in \mathfrak{L} \mid \{L,D\} \in \mathfrak{J} \wedge D \notin \mathfrak{L}_{sm}\}. \tag{2.4}$$

For the multi-body case, we express the net force-torque of a submodel as:

$$\sum_{L\in\mathfrak{L}_{sm}} {}_BX^L \, {}_L\phi_L = \sum_{L\in(\mathfrak{C}\cap\mathfrak{L}_{sm})} {}_BX^L \, {}_L\mathrm{f}_L^x + \sum_{L\in\mathfrak{L}_{sm}} \sum_{D\in\beth_{sm}(L)} {}_BX^D \, {}_D\mathrm{f}_{D,L}, \tag{2.5}$$

where ${}_L\mathrm{f}_L^x$ is the contact force-torque of link L expressed in link L frame, ${}_D\mathrm{f}_{D,L}$ is the force-torque that link D exerts on link L as seen by the FT sensor in between both links and $\mathfrak{C} \subseteq \mathfrak{L}$ is the subset of the links where contact force-torques are acting . Noting that in (2.2) and in (2.5) the only unknowns are the contact force-torques, the estimation problem may be solved rewriting these equations in the matrix form $Cx = b$, where $x = \sum_{L\in(\mathfrak{C}\cap\mathfrak{L}_{sm})} {}_L\mathrm{f}_L^x \in \mathbb{R}^u$ contains all the u contact unknowns, whereas $C \in \mathbb{R}^{6\times u}$ and $b \in \mathbb{R}^6$ are completely determined.

The estimation scheme takes into consideration the following three types of possible contacts:

- pure force-torque : ${}_L\mathrm{f}^x \in \mathbb{R}^6$, unknown vector corresponding to force and torque expressed in the link frame of contact L.
- pure force : $f^x \in \mathbb{R}^3$, unknown vector corresponding to a pure force and no torque.
- force norm : $\|f^x\| \in \mathbb{R}^1$, unknown assuming the pure force to be orthogonal to the contact surface.

The matrix C is built by adding columns for each contact according to its type. The columns associated to pure force-torques (C_w), pure forces (C_f) and pure force norm (C_n) are the following:

$$\begin{aligned} C_w &= \begin{bmatrix} {}_BX^L \end{bmatrix}, \\ C_f &= \begin{bmatrix} {}^BR_L \\ 0_{3\times 3} \end{bmatrix}, \\ C_n &= \begin{bmatrix} {}_BX^L \end{bmatrix} \begin{bmatrix} \hat{u}^x \\ 0_{3\times 1} \end{bmatrix}. \end{aligned}$$

where B is a common frame, in this case the base of the sub-model was selected, and $\hat{u}^x$ is the unit normal vector of the contact force-torque. The matrix C mainly depends on the contact location sensed by the skin. The 6 dimensional vector b is defined from (2.5) in the following way:

$$b = \sum_{L \in \mathfrak{L}_{sm}} {}_B X^L \, {}_L\phi_L - \sum_{L \in \mathfrak{L}_{sm}} \sum_{D \in \beth_{sm}(L)} {}_B X^D \, {}_D\mathrm{f}_{D,L}. \tag{2.6}$$

The vector b depends on kinematic quantities derived from whole-body distributed gyros, accelerometers, encoders and the FT sensors [44]. Once C and b have been computed, we can solve the equation $Cx = b$ for estimating contact force-torques.

When only a single contact acts on the sub-model, there are six unknowns for a system of six equations, therefore, the associated force-torque has a unique solution. Whenever two or more contacts are detected, the system admits infinite solutions and it is impossible to get a reliable estimate of the contact wrenches without imposing some constraints to the system. The adopted solution consists in computing the minimum norm x^* that minimizes the square error residual:

$$x^* = C^\dagger b$$

where $C^\dagger$ is the Moore-Penrose pseudo-inverse of C [30]. The above solution distributes equally the total contact force-torque among all contacts.

2.4.3 Joint Torque Estimation

Once an estimate of contact forces are obtained with the method described in subsection 2.4.2, internal force-torques can also be estimated with a standard Recursive Newton-Euler Algorithm (RNEA). The torque $\tau_{\{E,F\}}$ of the joint connecting link E and F comes from the projection of the joint force-torque on the joint motion subspace [129] :

$$\tau_{\{E,F\}} = \left\langle {}^F\mathrm{s}_{E,F}, {}_F\mathrm{f}_{E,F} \right\rangle = \left\langle {}^E\mathrm{s}_{F,E}, {}_E\mathrm{f}_{F,E} \right\rangle, \tag{2.7}$$

$$ {}_F\mathrm{f}_{E,F} = -{}_E\mathrm{f}_{F,E}, \tag{2.8a}$$

$$ {}_F\mathrm{f}_{E,F} = \sum_{L \in \gamma_E(F)} {}_F X^L \left({}_L\phi_L + {}_L\mathrm{f}^x_L \right), \tag{2.8b}$$

$$ {}_E\mathrm{f}_{F,E} = \sum_{L \in \gamma_F(E)} {}_E X^L \left({}_L\phi_L + {}_L\mathrm{f}^x_L \right), \tag{2.8c}$$

where $\gamma_E(F)$ is the set of the links belonging to the sub-model starting at link F, given E as a base link, ${}^{E}s_{F,E}$ is the mapping between the relative 6D velocity of the two bodies connected by the joint and the joint velocity known as *joint motion subspace vector* [37, 129].

2.5 Robots dynamic performance

While is true that some robots are now able to walk, jump, run and even parkour. These behaviors are still not achieved in a consistent reliable way. The most known example is the robot Atlas' videos released by Boston Dynamics, Fig. 2.7. As stated by Boston Dynamics' CEO Marc Raibert, "In our videos, we typically show the very best behavior. It's not the average behavior or the typical behavior. And we think of it as an aspirational target for what the robots do." These type of dynamic behaviors establish different rapidly changing contacts with the environment generating impacts making relevant the dynamics response of the sensor. A situation where is useful to have force-torque sensing is when a contact is established, also called collisions. Fix based robots are able to achieve dynamic behaviors such as handle unexpected collisions to some extent [81] and even cooperate with humans [117]. They achieve this by exploiting force-torque sensing to estimate contact forces and measure or estimate joint torques. Multiple schemes for handling collisions are presented in a survey on robot collisions [51]. The initial problems to be solved in this schemes is the detection of contacts, followed by the location of contacts and the identification of contacts. This can be rephrased as realize a contact happened, understand where it happened and measure the force of the contact. Nonetheless, these schemes are only suitable for robots with their base fixed to the ground.
For floating base systems is possible to obtain and use collision related information using FT sensors, joint torque sensors in addition to encoders, and gyroscopes [137]. In this scheme, an improvement in the force-torque sensing will directly create an increase in the performance of the scheme. There are some robots with only one kind of force sensor like the iCub, described in Section A.1, or with none like Pepper [17]. As a result, this scheme can not be applied directly to these robots.

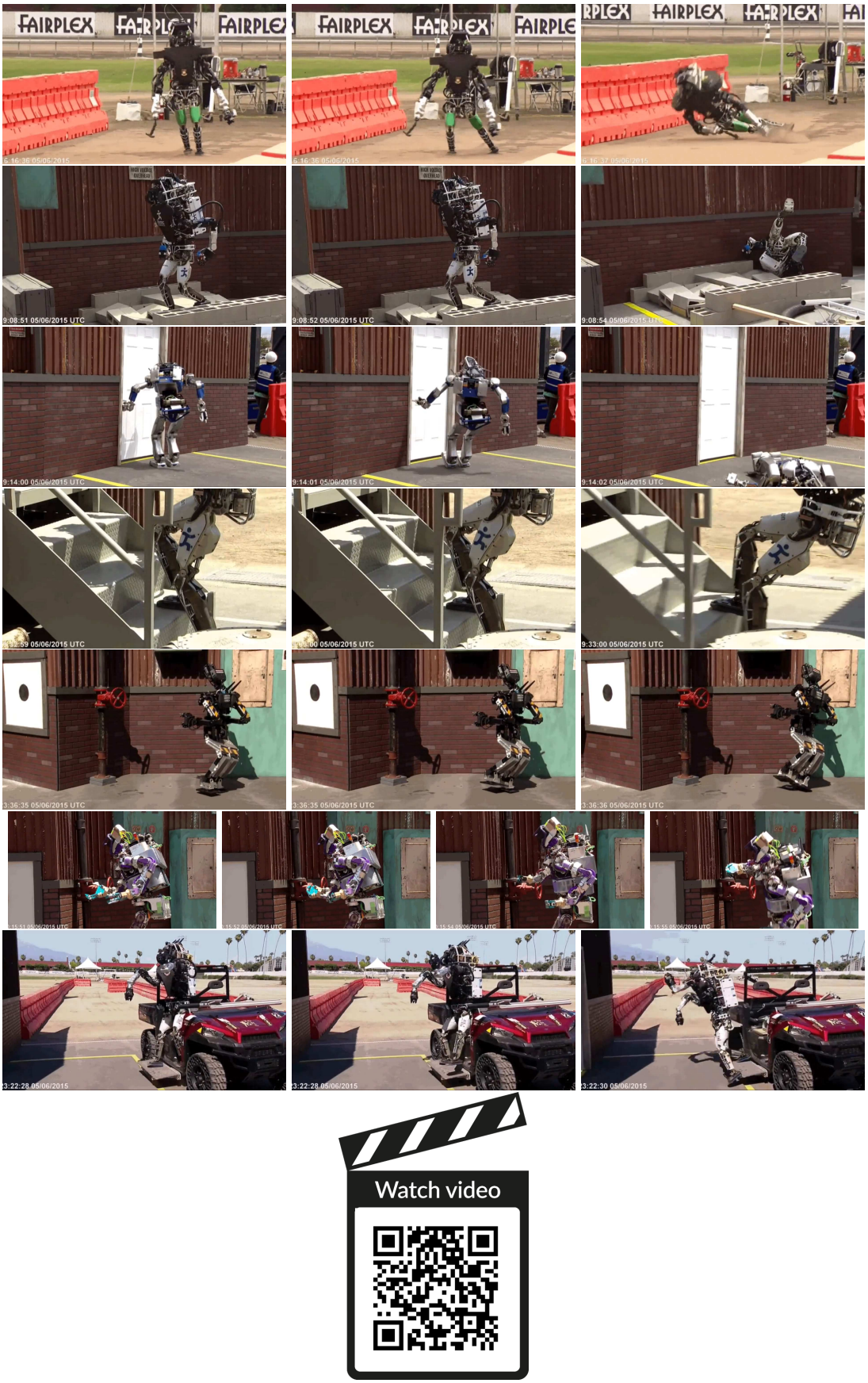

Fig. 2.6 DARPA Challenge 2015 failures.

Despite the amount of theoretical background to exploit force-torque sensing, floating base robots in real scenarios still struggle with handling interactions with the environment or other bodies. A good example is the results from the DARPA Robotics Challenge Finals in June 2015 [10, 27, 60, 26].

During the challenge, most of the teams could not take full advantage of having FT sensors. The reason why no other extra objects where used for support or stabilization is mentioned to be the the bad quality of the wrist FT measurements [10]. The Boston Dynamics ATLAS' FT sensor measurements were only used as binary contact sensors by the IHMC and MIT teams [27]. It was mentioned that having more FT sensing information in the form of full six axis FT sensors at the ankle would have allowed to improve results [26]. Examples of failed attempts are shown in Fig. 2.6. Different type of failures can be seen. Being unable to understand if the robot has made contact with the environment (being the ground or a handle). Discerning if the contact is stable enough to shift the weight of the robot to the contact. Problems arising from unexpected contacts can easily happen in reduced spaces. Although there are many reasons for the different failures, the situations previously described are examples of situations in which accurate FT sensing information can provide crucial knowledge to increase the probability of successfully perform the tasks.

Fig. 2.7 Boston Dynamics' Atlas doing parkour.

The fact that force-torque sensors are affected by mounting issues [130, 8] or temperature drift [54, 127, 113], reduces the reliability of these sensors and as a consequence the performance and repeatability of dynamic behaviors in robots. Poor performance of six axis FT sensors have been reported in the literature. Unkown errors in the measured magnitude [13, 52]. Lower performance than other FT solutions like force plates has been mentioned [105].
An example of errors due to bad FT measurements can be seen in Fig. 2.8. The full video can be seen using the QR code or clicking in this link . In this experiment, the contact forces are estimate using the information from six axis FT sensors and the algorithm described in Section 2.4. It can be seen that even if the algorithm is able to detect contact forces while the

robot is not moving. When the robot starts moving contact forces that do not exist appear. Upon inspection it was revealed that the measurements of the FT sensors were not very accurate. Given the performance of six axis FT sensors attempts to improve the measurements. Some rely on redundant sensors [133]. Others rely on reconstructing the ground reaction force through kinematics and IMU measurements. Then use this information to create a Virtual Force Sensor that is constantly compared with FT measurements to detect and recover faulty measurements [52].

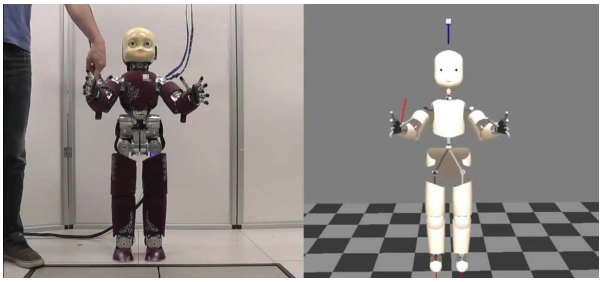

(a) Algorithm correctly detecting contact forces.

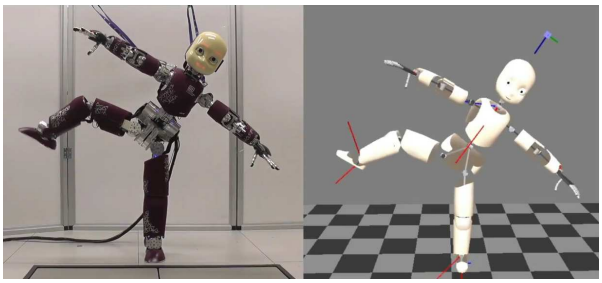

(b) Algorithm incorrectly detecting contact forces.

(c) QR code for full video.

Fig. 2.8 Contact Force Estimation using algorithm in Section 2.4.

A common strategy in FT sensors to reduce the effect of drift is to remove the bias just before a change in the load is expected. Robots that have their base fixed to the ground can

benefit from this method to some extent. Instead in floating base robots, this is not practical. Most of the time the sensors themselves are used to detect unexpected contacts so the time of collision is not known *a priori*. Besides, the main function of the sensors is to measure the actual force applied or received by the robot. In a scenario in which the robot is already in contact with a surface, removing the bias will make the value of the measured FT incorrect.
From the literature, it can be seen that six axis FT sensors are in more need of improvement than joint torque sensors. It is worth to notice that contact joint torques can be completely reconstructed from the knowledge of the contact forces and the robot model. On the other hand, there are some contact forces that might not be observable when estimating them through the joint torques. As a result, a very promising solution is to increase the performance of force-torque sensors already mounted in the robots while allowing them to cope with sources of drift such as temperature. Typically, in fixed based robots they were used in slow and short motions in industrial applications. Fixed based robots have less chances of encountering changing environments. When used in floating base robots, these sensors might be subjected to a very wide range of motions be it slow and short or fast and wide. They might also experience impacts and inertia constantly changing with the robot configuration. Potentially floating base robots can be used outdoors and be deployed to disaster areas. This means that the environmental conditions might be really different from the fixed base robots. All this should be taken into account when seeking to improve a sensor performance.
Even if the principles of force-torque sensors are well known, there are many things that can become uncertain during the manufacturing process. This complicates the direct use of the theory to derive the relationship between the input of the sensor and the desired output from a sensor. It is possible to obtain force-torque information in more indirect ways by profiting from the relationship forces and torques have with other physical quantities. An example would be the estimation of a motor torque through the current and the model of the motor. Another example is the estimation of forces due to the movement of a body by knowing its mass and acceleration. In fact, these relationships can be exploited to adjust the performance of a sensor by estimating the relationship between the stimuli and the digital output of the sensor. This is what the calibration is for. Chapter 3 explains what calibration is and how is done. It also covers some state of the art in the calibration of FT sensors and tactile arrays.

Chapter 3

Calibration Procedures

Understanding how FT sensors are placed in robots and a general idea of the uses they have in these robots allows to shape the requirements of the performance of the sensor. A sensor converts a stimuli to an electrical signal. The knowledge of the working principles of the sensor may allow to calculate the how the stimuli is converted to the output signal. It is possible that the stimuli have no direct relationship to the electrical signal and intermediate steps are needed. Nonetheless, from the perspective of the user, the sensor should receive the selected stimuli and give a corresponding measurement. Even in cases where the working principle of the sensor is known, reality might differ due to manufacturing or environmental factors. Furthermore the calibration should consider the expected use of the sensor to provide more accurate measurements. In this Chapter, the way to allow a sensor to provide accurate measurements despite these factors is addressed.

3.1 Mathematical Modeling of a Sensor

There is a theoretical input-output (stimulus-response) relationship for every sensor. If a sensor is ideally designed and fabricated with ideal materials by ideal workers working in an ideal environment using ideal tools, the output of such a sensor would always represent the true value of the stimulus. This input-output relationship is called transfer function. In control theory, the transfer function $H(s)$ is often expressed as the ratio between the input function $X(s)$ and the output function $Y(s)$, $H(s) = \frac{Y(s)}{X(s)}$. Nonetheless, for the discussion that follows regarding sensor calibration it is enough to use a general formulation in the form of:

$$E = h(s), \tag{3.1}$$

where s is the stimulus, $h(s)$ is the transfer function and E is the electrical response.

Ideally, the transfer function can be based on a physical or chemical law that forms a basis for the sensor's operation. It is possible that more than one law is required to map all the working principles of the sensor. If such a law can be expressed in the form of a mathematical formula, often it can be used for calculating the sensor's inverse transfer function by inverting the formula ($s = h^{-1}(E)$).

In reality, a sensor does not perfectly comply with the mathematical formula of the phenomena it is based on. Too many ideal conditions are required for this to happen. Besides, readily solvable formulas for many transfer functions, especially for complex sensors, does not exist and one has to resort to various approximations of the direct and inverse transfer functions. Common approximation functions are [43]:

- Simple Models
- Linear Regression
- Polynomial Approximations
- Linear Piece-wise Approximation
- Spline Interpolation
- Neural Networks

The relationship between the change of the phenomena to an electrical value for a specific sensor is obtained through a process called calibration. The objective of the calibration process is to obtain the parameters of the chosen approximation function for the specific sensor. These parameters are referred to as calibration values or calibration parameters.
The accuracy of the sensor is then a result of the calibration process. It requires the mathematical model of the phenomena (or a good approximation) and known stimuli paired with the corresponding sensor's response.
A pair of known stimuli with the sensor response is called a calibration point. A set of calibration points is a calibration data set. The stimuli and sensor response are also called reference data and raw measurement respectively.

3.1.1 Functions Based in Simple Models

It is desirable that a transfer function has a small number of parameters that require estimation. This is the reason why using simple models is convenient. Of course, the choice of the model depends on how good they fit the response of a particular sensor.

Linear Function

The simplest possible transfer function is linear. The math model can be expressed as :

$$E = Cs + O, \tag{3.2}$$

where O is the value of E at $s = 0$, typically called offset or bias; C is the slope of the line, sometimes referred to as sensitivity. The graphical representation can be seen in Fig. 3.1. Eq. (3.2) assumes the possibility of evaluating the sensor at $s = 0$ value. This might not be possible in all cases (think of a temperature sensor in Kelvin scale). For such cases it can be shifted to a known stimulus s_0 using the following equation:

$$E = E_0 + C(s - s_0), \tag{3.3}$$

where E_0 is the known response at s_0. For this linear model, the inverse transfer function $h^{-1}(E)$ has the following form:

$$s = \frac{E - E_0}{C} + s_0 \tag{3.4}$$

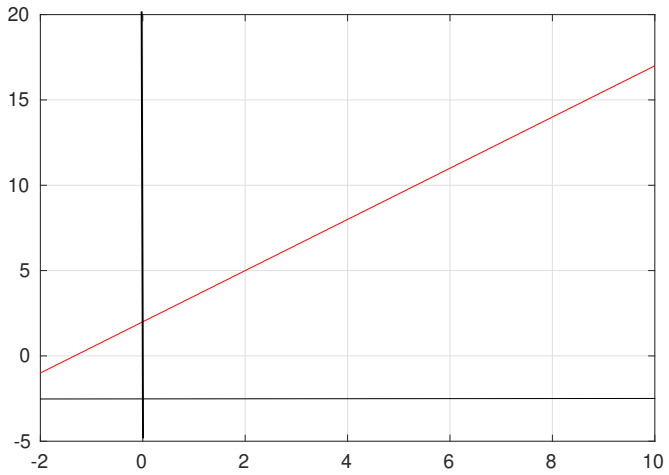

Fig. 3.1 Graphical representation of linear model.

Non linear Functions

A nonlinear transfer function can be approximated by a nonlinear mathematical function. The three main functions based in nonlinear models are the logarithmic, exponential and power

Function	$h(s)$	$h^{-1}(E)$
logarithmic	$C\ln+Os$	$e^{\frac{E-O}{C}}$
exponential	Oe^{ks}	$\frac{1}{k}\ln\frac{E}{O}$
power	Cs^k+O	$\sqrt[k]{\frac{E-O}{C}}$

Table 3.1 Simple nonlinear transfer functions.

functions. Their mathematical equations and inverse transfer functions can be seen in Table 3.1. Its corresponding graphical interpretations can be found in Fig. 3.2

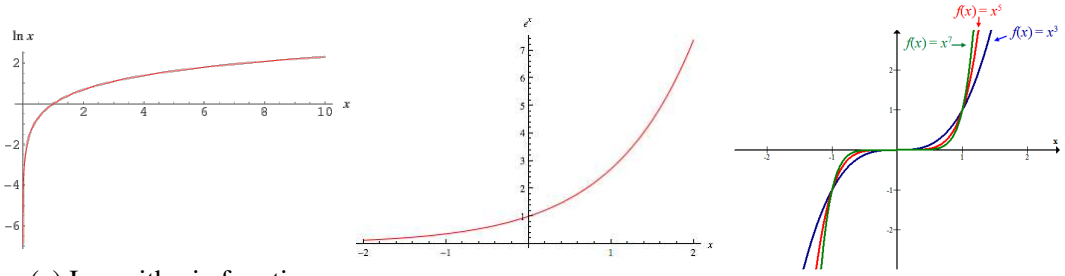

(a) Logarithmic function. (b) Exponential function. (c) Power function.

Fig. 3.2 Graphical represenation of nonlinear transfer functions.

3.1.2 Linear Regression

As the name implies it attempts to find the transfer function using assuming a linear model. It is to be distinguished from the linear model in the fact that this is not a deterministic approach but a statistical approach. This means that it will attempt to find the best linear function that fits the data, even if not all calibration points are on the found line. An example can be seen in Fig. 3.3. The use of linear regression helps to cope with random errors that may appear in the calibration process.

The typical method for performing linear regression comes from the least squares algorithm. The formulation of the least squares problem is:

$$\arg\min_{C} \frac{1}{N}\sum_{i=1}^{N} \|s_i - CE_i\|^2 \tag{3.5}$$

The solution to this problem is straightforward and well known in statistical literature. It minimizes the sum of squared residuals. The calibration parameters are the solution to the least

square problem and have the following form [75]:

$$C = (E^T E)^{-1} E^T s. \tag{3.6}$$

Least square can be extended for solving for multiple variables. Multiple regression is an extension of simple linear regression. It is used when we want to predict the value of a variable based on the value of two or more other variables. Each variable can be considered as a different sensor. There are other extensions to the least squares formulation for nonlinear cases, but those are beyond the scope of the current thesis.

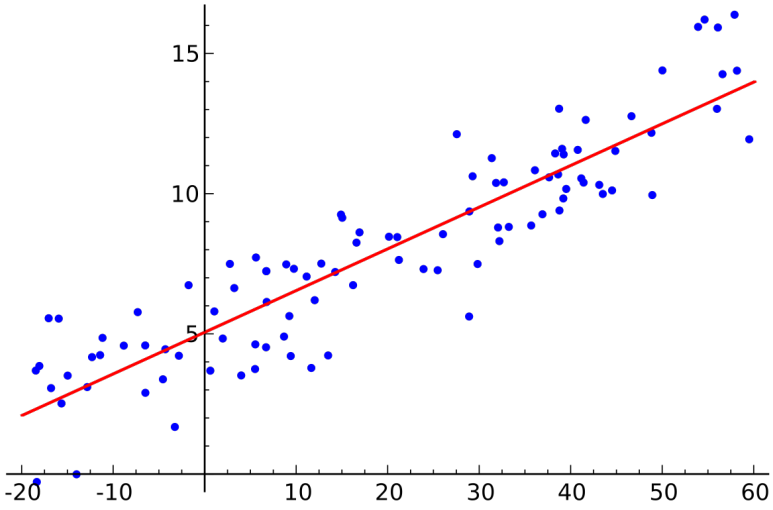

Fig. 3.3 Graphical representation of linear regression.

3.1.3 Polynomial Approximations

Any continuous function, regardless of its shape, can be approximated by a power series, this is also called polynomial approximation. A polynomial approximation function takes the following shape:

$$E = D_0 + D_1 s + D_2 s^2 + \ldots D_n s^n, \tag{3.7}$$

where D_i are the coefficients corresponding to the n-th power or polynomial degree. These parameters allow to shape the curves to obtain $h(s)$. For polynomial approximations is more complex to find $h^{-1}(E)$ starting from $h(s)$. For this reason is common to directly estimate the coefficients of $h^{-1}(E)$:

$$s = C_0 + C_1 E + C_2 E^2 + \ldots C_n E^n, \tag{3.8}$$

where C_i are the calibration parameters corresponding to the n-th power.
An example can be seen in Fig. 3.4. It can be observed that in this case increasing the degree of the polynomial increases the fitting of the data. This depends on the underlying behavior of the system. It is quite common that a real system suffers from noise. In the presence of noise, increasing the polynomial degree risks over-fitting the data, preventing from getting a good generalized approximation function.
A way to solve the polynomial fitting problem is to use multiple regression. Where the other variables are generated by elevating the sensor response up to a n-th degree. Least squares can be used since $h^{-1}(E)$ is linear in terms of the calibration parameters.

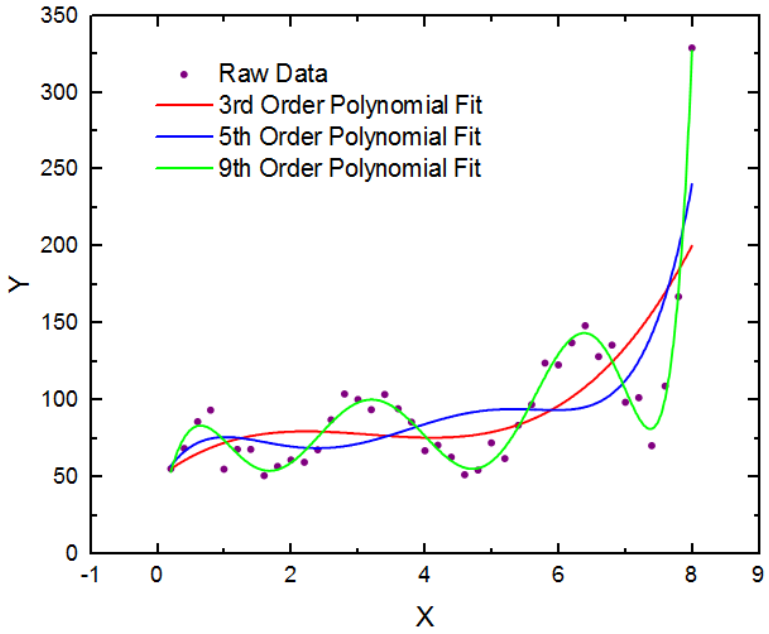

Fig. 3.4 Graphical representation of polynomial approximation using different powers.

3.1.4 Linear Piece-wise Approximation

The idea behind it is to break up a nonlinear transfer function of any shape into sections and consider each such section being linear. Curved segments between the sample points demarcating the sections are replaced with straight line segments, thus greatly simplifying the behavior of the function between the points. This can also be seen as a polygonal approximation of the original nonlinear function. An example is shown in Fig. 3.5.

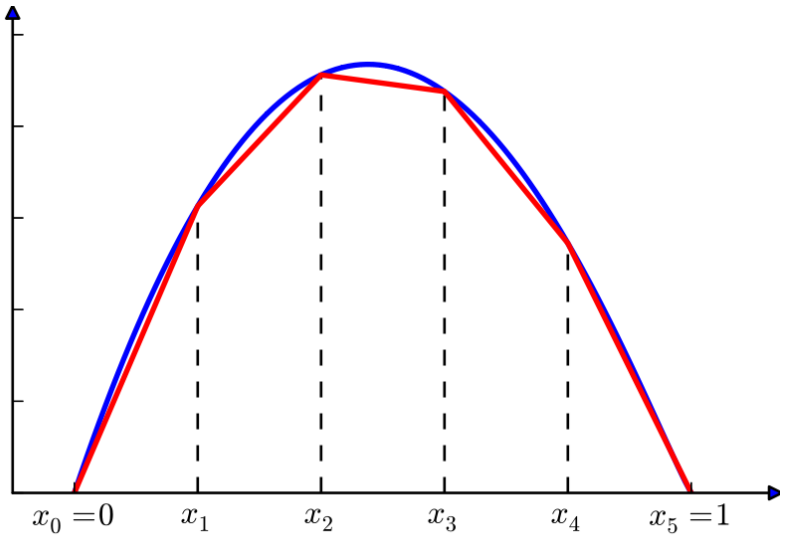

Fig. 3.5 Graphical representation of piece-wise linear approximation.

3.1.5 Spline Interpolation

Approximations by higher order polynomials (third order and higher) have some disadvantages; the selected points at one side of the curve make a strong influence on the remote parts of the curve. This deficiency is resolved by the spline method of approximation. In a similar way to the linear piece-wise interpolation, the spline method uses different third-order polynomial interpolations between the selected experimental points. The graphical representation can be found in Fig. 3.6.

3.1.6 Neural Networks

An artificial neural network, or just neural network, is a mathematical model which models itself after the human brain. Similar to the brain's neurons, it has unit blocks also called neurons or perceptrons. This is normally the most complex approximation function because one or more parameters for each neuron has to be estimated (or learned). Nonetheless, it has the potential to approximate any continuous function. The network learns an input-output mapping (transfer function) with a method called supervised learning. A single neuron is mathematically represented as:

$$y = \phi\left(\sum_{i=1}^{N} w_i x_i + b)\right), \tag{3.9}$$

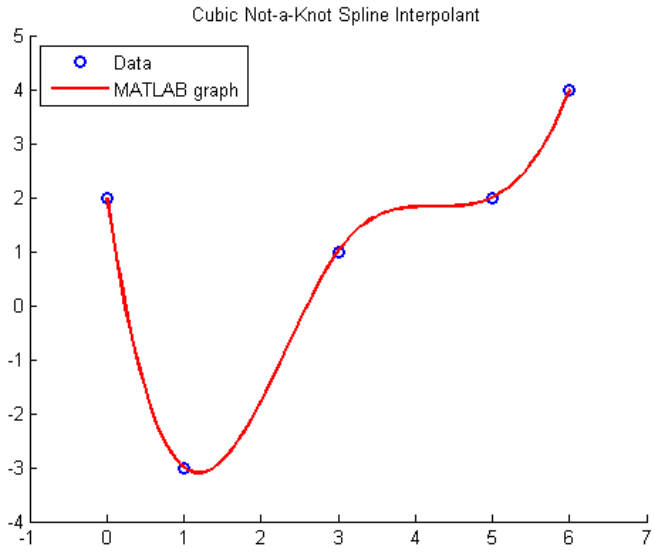

Fig. 3.6 Graphical representation of spline interpolation.

where x_i are the inputs to the neuron, w_i are the weights of each input, b is the bias, ϕ is the activation function and y is the output of the neuron. Each input weight and the bias needs to be learned. A graphical representation of neuron can be seen in Fig. 3.7a

In the mathematical theory of artificial neural networks, the universal approximation theorem states [24] that a feed-forward network with a single hidden layer (Fig.3.7b) containing a finite number of neurons with arbitrary activation function are universal approximators.

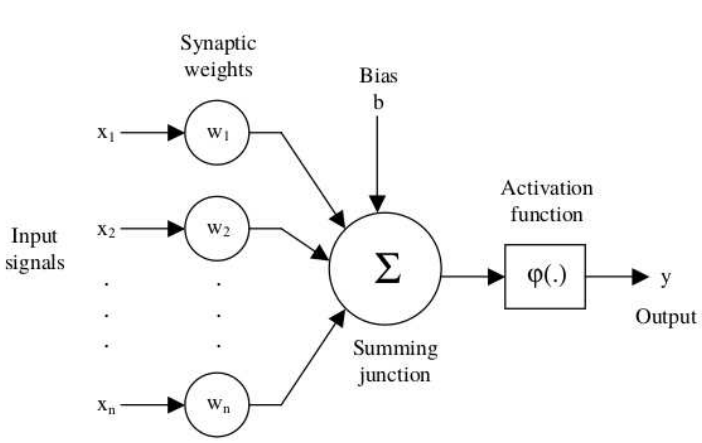

(a) Graphical representation of a neuron.

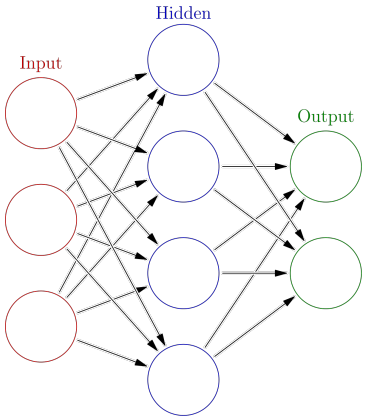

(b) Feed-forward network with a single hidden layer.

Fig. 3.7 Graphical represenation of a neural network.

Neural networks have the potential to approximate any continuous function, but the physical meaning of the solution is usually lost. Neural networks have become a standard tool to tackle problems where we want to make preditions without following a particular algorithm or imposing structure on the available data. Most work to date has focused on the efficiency or quality of predictions of neural networks, without an understanding how they solve the problem [58]. They are often applied as a black box, which from a results point of view, has no contradiction with the aim of calibrating a sensor. Neural Networks is an active research field in its own. Providing deeper knowledge of the topic goes beyond the scope of the thesis.

Independently from the mathematical model, calibration procedures can be classified depending on the place the calibration data set is acquired. If the calibration data set is acquired in the system (or structure) in which is meant to be used, it is referred to as *in situ* calibration. Instead, if the sensor is calibrated in a structure then removed and mounted somewhere else for its use, it is refferred to as *ex situ* calibration.

3.2 Factors that affect sensor accuracy

Accuracy is defined as the maximum difference between the actual value and the sensor's output. Given a sensor design, substantial reductions in the measurement error, can be achieved only by using more sophisticated technologies, materials and components in the construction of the sensor, and finer models of the structure, or more accurate instrumentation for strain measurement and calibration. An improvement of these factors with respect to present sensors is therefore achievable by increasing their cost. However, there are absolute upper bounds to possible reduction of source errors set by present technological state-of-art, and by inherent measurement accuracy limitations.

The right approximation function can be chosen from knowledge of the working principles, but this alone does not ensure the accuracy of the sensor. During calibration, data from the sensor response is mapped to match the reference stimuli. The accurate knowledge of the reference data value coupled with the right approximation function warrants the future performance of the sensor. A factor that needs to be taken into account when calibrating is the expected use of the sensor this may define the range values of the reference stimuli. Other factors include errors during the acquisition of the calibration data. Lastly, conditions during calibration may be different than the conditions in which the sensor is actually used, this may have unforeseen or undesirable effects on the sensor. An ideal calibration procedure should take all these factors into account.

3.2.1 Full Scale and Resolution

All elements in the sensing module provide their own limitations. The sensing element has many design choices. Some of which include the possible range of the sensor based on the elastic limits of the material, the displacement response to a force which can help determine the stiffness of the resulting sensor and its sensitivity.
On the other hand, the combination of the amplification stage in the signal conditioning and the ADC number of possible conversion values place another set of limitations on the sensing module in terms of full-scale and resolution. Full-scale for an analog output is the algebraic difference between the electrical output signals measured with maximum input stimulus and the lowest input stimulus applied. For a digital output, it is the maximum digital count the ADC can resolve for the absolute maximum input [43]. The resolution defines the smallest voltage change that can be measured by the ADC. The number of possible conversion values depends on the number of bits in the output of the ADC called bit_{size}. These elements can be considered as the most limiting factors of the sensor since they are typically selected to be equal or under the limits of the sensing element.
The amplification stage can be characterized by a gain value g_a which is the amplifying factor of the signal. The full-scale is then the difference between the stimuli that generate the maximum voltage value s_{max} and the stimuli that generate the minimum voltage value s_{min} using a selected gain g_a for a given sensing element $Sens_{element}$. Reaching the maximum or minimum value is called saturation. The full-scale FS can be expressed as:

$$s_{max} = h^{-1}(E^{ref}_{max}|g_a, Sens_{element}) \tag{3.10}$$

$$s_{min} = h^{-1}(E^{ref}_{min}|g_a, Sens_{element}) \tag{3.11}$$

$$FS = s_{max} - s_{min} \tag{3.12}$$

where E^{ref}_{max} is the maximum voltage value in V, E^{ref}_{min} is the minimum voltage value in V. The full-scale is given in the units of the phenomena that is measured. The resolution of the ADC is the same as the smallest step size and can be calculated by dividing the reference voltage by the bit_{size}. Since the reference voltage determines the full-scale of a sensor, the sensor resolution is then:

$$res = FS/bit_{size} \tag{3.13}$$

The difference between the smallest and largest physical inputs that can reliably be measured by an instrument determines the dynamic range of the device [141]. For a digital output is determined by the value at saturation and the resolution of the sensor. A change in the stimuli under the resolution value of the sensor will not be measured correctly. Therefore, the resolution

affects also the accuracy of a sensor. The resolution can be improved by either reducing the full-scale or augmenting the bit_{size}. So the accuracy of the sensor can be improved by modifying $Sens_{element}$, g_a or bit_{size}. The value of g_a can be made variable without requiring major changes in the sensor even if it implies reducing the full-scale. Any change in the dynamic range of a sensor modifies the transfer function and requires a new calibration of the sensor.

3.2.2 Notes on acquiring calibration data

Ensuring the data used for calibration can be trusted is fundamental for a good performance of the sensor. Therefore, it is crucial to reduce the sources of uncertainty in the reference stimuli during the calibration procedure. Some guidelines for data acquisition are proposed based on the acquired experience. Although errors might still exist during a careful calibration procedure, the following guidelines can help reduce uncertainty:

- The data of the reference stimuli should be of equal or better accuracy than the intended accuracy of the sensor.
- The procedure should take place in a controlled environment.
- The least amount of human intervention helps reducing variability.
- Avoid any interference of external factors during data acquisition.

When something goes wrong during the calibration procedure is usually the case that the whole procedure has to be repeated adding time to a typically time-consuming task. Therefore making the procedure easily repeatable tends to be a desirable feature. Having a way to understand if the acquired calibration data set is useful or not might prevent from performing erroneous calibration. This increases calibration efficiency.

3.3 Calibration of Six Axis Force-Torque Sensors

A force sensor does not measure the force directly. Measuring a force is the result of converting other physical phenomena that varies in response to force into an electrical signal. The relationship between the change of the phenomena to an actual force value is obtained through the calibration procedure.
The most common phenomena used in force-torque sensors is the change in resistance of silicon due to strain. In more technical words, the piezoresistive response to strain of semiconductor material. This material also changes resistance with temperature. Because of this, depending

on the calibration procedure, the sensor might suffer from temperature drift. Which is the undesired change of measurement due to changes in temperature.
For sensors based in metallic foil or silicon strain gauge, the sensor is designed such that the resulting deformation in the structure of the sensors are inside the linear section of the sensing material for the specified range. Because of this, a linear relationship between deformation and forces can be assumed. For single-axis force sensor, it is simple to use an array of strain gauges in a Wheatstone Bridge configuration to perform temperature compensation by itself. Fulfilling the requirements to achieve the same in a multi-axis FT sensor at hardware level complexifies the design, increases the number of components needed and the cost.

3.3.1 Mathematical model

There are two physical laws at play in strain gauge force sensors. One is common to all kinds. It is the relationship between the deformation of a spring and forces, it is the Hooke law of elasticity, described in more detail in Section1.2.

$$f = k\Delta x, \tag{3.14}$$

where f is the force value in N, k is a constant of the material $\frac{\mathrm{N}}{\mathrm{m}}$ and Δx is the displacement (or strain) in meter. It is valid as long as the material does not reach plastic deformation. The other principle depends on the type of sensing technology. For semiconductor strain gauges it is the piesoresistive effect. As mentioned in Section 1.3.1, the model is the linear function:

$$R = R_o(1 + S_\varepsilon \varepsilon), \tag{3.15}$$

where R is the resistance value in Ω, S_ε is the gauge factor of the conductor, R_o is the resistance with no stress applied in Ω. Combining both physical effects gives the following transfer function:

$$R = R_o(1 + S_\varepsilon \frac{f}{k}) \tag{3.16}$$

Therefore the most used model for predicting the force-torque from the raw strain gauges measurements of the sensor is a linear model. The inverse function is:

$$f = \frac{(R-R_0)k}{S_\varepsilon R_0} \tag{3.17}$$

$$= \frac{Rk}{S_\varepsilon R_0} - \frac{k}{S_\varepsilon} \tag{3.18}$$

$$= cR - O, \tag{3.19}$$

where

$$c = \frac{k}{S_\varepsilon R_0}$$
$$O = \frac{k}{S_\varepsilon}.$$

Considering possible errors during the calibration procedure linear regression is the most suitable approximation function. Multi-axis force-torque sensors usually contain multiple strain gauges, each of them can be seen as a separate sensor. Because of this, multiple regression is a valid option for this kind of sensors. Therefore each force axis will be calibrated using the information from all strain gauges,

$$f_i = c_1 R_1 - O_1 + c_2 R_2 - O_2 + ...c_m R_m - O_m, \tag{3.20}$$

where f_i is the force in the i-th axis in N or N m depending on the axis, R_m is the digital response of the m-th strain gauge in bit counts, c_m is the slope of the linear model of the m-th strain gauge in $\frac{\mathrm{N}}{\mathrm{bit}}$ and O_m is the bias of the m-th strain gauge. The orientation of f_i with regards to the m-th strain gauge will change the value of k required. It depends on the strain being normal, shear or a combination of both. As a result, the array of c_m coefficients C_m and O_m will be different for each i-th axis. Taking this in consideration, the approximation function for these sensors has the following form:

$$\mathrm{f} = Cr + o \tag{3.21}$$

where $\mathrm{f} \in \mathbb{R}^6$ are the 6D forces, $C \in \mathbb{R}^{6\times m}$ is the calibration matrix in $\frac{\mathrm{N}}{\mathrm{bit}}$, $r \in \mathbb{R}^m$ are the raw measurements (sensor's response in bit counts) and $o \in \mathbb{R}^6$ is the offset which is also a 6D force vector. Both the calibration matrix C and the offset o are unknown and need to be estimated.

3.3.2 Calibration procedures

The typical calibration procedure considers first identifying the offset when no load is applied on the sensor. Then, carefully place some weights in specific positions to have well known gravitational forces and torques in order to span the space of the sensor. In order to resolve the coupling effects, is necessary to have calibration points with as many orientations of the force vector as possible based on the sensor's coordinate system. In other words, have as many differnent points as possible in the 3D force space. If the calibration data sets are obtained when the multi-axis forces and torques are applied to the sensor, the coupling effect can be solved [95]. The calibration data should ideally be a representative data set of what the sensor will be subjected to. The methods for obtaining the calibration matrix have been thoroughly studied and although many methods exist, solving with least squares remains the

most popular [19].
In standard operating conditions, a decrease in the effectiveness of the calibration may occur in months. Leading companies for FT sensors [11, 142] recommend to calibrate the sensors at least once a year. The calibration done by the manufacturer usually implies that the sensor must be unmounted, sent back to them and then mounted again. The typical callibration procedure is a quasi-static calibration of the sensor. Dynamic calibration of these kind of sensors has rarely been investigated due to the complexity involved [78]. Few attempts have been done to model and compensate for dynamic effects [78, 14, 39, 148]. Usually this calibration procedures match one of three categories: frequency response, impact response or step response. In general they highlight the difficulty of a repeatable dynamic calibration procedure and do not consider complex load cases.

Ex Situ Calibration Procedures

The task of creating equipment to carry out the calibration with high accuracy is equal in importance to the problem of the design of the FT sensor [151].
For simplifying the time-consuming procedure of careful load placing, some specialized structures have been designed [134, 140, 16, 126]. Even with the help of these specialized structures, human intervention is used in every single calibration point since the change of load is manual.

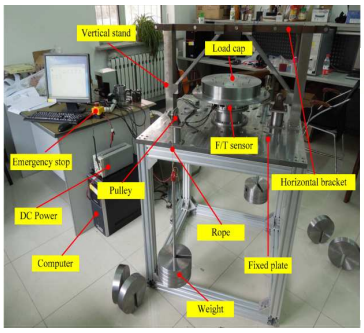

(a) Using specifically designed structures [126].

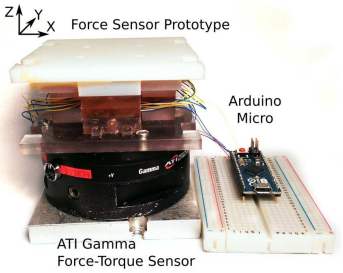

(b) Using another sensor [50].

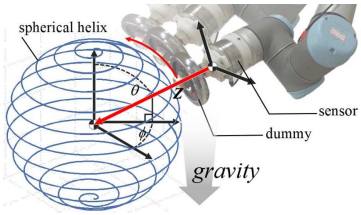

(c) Using robotic arm [96].

Fig. 3.8 Examples of *ex situ* methods.

Some have used complicated structures for the calibration of the sensor, with a combination of four joints with two DoF each and four pulleys [151]. This structure uses a complementary device to change the orientation of the sensor and therefore the application of the load on the sensor. This allows calibrating with less human intervention. The actual mechanism to change the orientation of the sensor is not described.

Others have taken advantage of six DoF robotic arm to span as many orientations of the sensor as possible with a known mass [95, 96]. Even if the sensor is mounted on a robot, it is strictly used as a medium to obtain the calibration data sets, not the working destination of the sensor. In other cases, a previously calibrated sensor is used as reference [36, 94, 3, 50]. This has the disadvantage of trusting on the calibration of another sensor which might not be accurate.

In Situ Calibration Procedures

FT sensors are prone to change performance once mounted in a mechanical structure such as a robot [130, 8]. Different methods have been developed to re-calibrate the sensors once mounted. These *in situ* methods allow to perform the calibration in the sensor's final destination, avoiding the decrease in performance that arises from mounting and removing the sensors from its working structure. The relevance of calibrating *in situ* has become evident, making *in situ* calibration part of the service provided by FT sensor companies [71].

To the best of our knowledge, the first FT sensor *in situ* calibration method exploited the topology of a specific kind of manipulators equipped with joint torque sensors. They assumed the center of mass of the wrist and the objects grasped are known and aligned with the z-axis of the sensor. Using three different sets of masses and some predefined positions they estimate the inverse calibration matrix with least squares. Then an approximate relationship to do the pseudoinverse is applied. The torque measurements in a specific position are exploited to complement the calibration points [120]. Another *in situ* calibration method for FT sensors can be found in [112]. But, the use of supplementary already-calibrated force-torque/pressure sensors, impairs this method since those sensors are prone to be affected by the mounting procedure, propagating the error from sensor to sensor. Some calibrate the sensor mounted in their final position by designing a calibration bench that accommodates the sensor and the mounted structure [146]. This requires the design of a particular structure and the mounting and dismounting of the whole part to calibrate the sensor. Another approach calibrates a FT sensor in a robot leg. The calibration forces and torques are induced manually by a human user through the four handles (black cylinders) of the tilt and pan plate mounted on top of the reference sensor [25]. Even with the novel approach for online calibration, it requires the cooperation of a human and a reference sensor.

Another method has shown that six axis FT sensor can be calibrated based on the shape from motion method with a complex algorithm. This requires the use of three different sets of weights and a minimal setup with a fixed pulley. It requires to calibrate the sensor three times per load so in total nine calibration data sets [125].

Some methods rely on adding other external sensors, such as accelerometers, to obtain a ground truth [130]. This translates the source of error to the accuracy of the accelerometers and

measurement of the transformation matrix between the sensor frames.
In all of these methods, the effect of temperature is either not considered or carefully controlled when calibrating without accounting for changes in the working conditions.

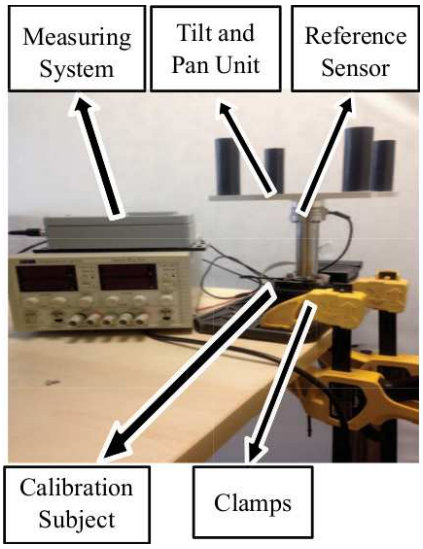

(a) Pan Tilt mechanism on top of foot [25].

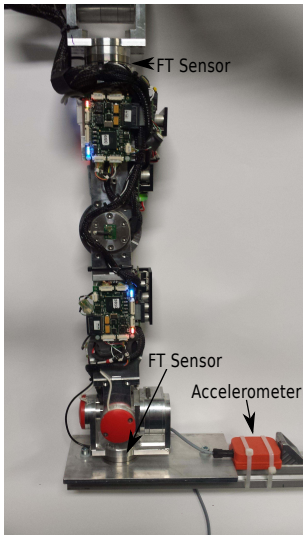

(b) Using accelerometers [130].

Fig. 3.9 Examples of *in situ* calibration.

Measurement Accuracy and Resolution

In most of FT sensors, the accuracy is calculated with respect to the full-scale of the sensor. The resolution of the measurements is conditioned by the ADC converter. By changing the value of the gains is possible to affect the limit at which the ADC reaches saturation. As a consequence, the sensor range and resolution are changed. Therefore a higher gain implies lower range and better resolution. With better resolution the calibration of the sensor can be more accurate. By having the option of changing the gains is possible to use the same sensor while optimizing the calibration for a specific range.

3.4 Force Calibration of Tactile Sensor Arrays

Similar to force-torque sensors, in tactile sensor arrays, the Hooke law allows to relate the displacement to a force. The other physical phenomena depend on the technology used. Since a calibration considering piesoresistive effect is described in the previous section, in this sec-

tion the capacitive effect is used. This happens to aligns with the available technology in the lab.

3.4.1 Mathematical model

For tactile sensor arrays, the shape of the capacitor can be assumed to be flat. As mentioned in Section 1.3.2, for flat capacitors the capacitance Ca in F can be calculated as:

$$Ca = \kappa\varepsilon_0 \frac{A}{d}, \tag{3.22}$$

where κ is the dielectric constant of the material in $\frac{\mathrm{F}}{\mathrm{m}}$, ε_0 is a constant if the sensor were found in vacuum also in $\frac{\mathrm{F}}{\mathrm{m}}$, A is the area of the plates in m^2 and d is the distance between the plates in m.
Considering the Hooke law described in eq. (3.15) and the capacitance for a flat capacitor described in eq. (3.22), the transfer function is built on the change of capacitance due to the displacement of the plates when a force is applied as follows:

$$Ca = \kappa\varepsilon_0 \frac{A}{d_0 + \Delta d}, \tag{3.23}$$

where Ca is the capacitance after a displacement and d_0 is the original distance in m. Using eq. (3.15) and knowing there will only be forces induced by compression the final form of the transfer function is:

$$Ca = \frac{\kappa\varepsilon_0 A}{d_0 + \frac{-f}{k}} \tag{3.24}$$

An example of the behavior of this transfer function can be seen in Fig. 3.10. It behaves like an negative logarithmic funciton. This way the inverse transfer function is:

$$f = \frac{\kappa\varepsilon_0 Ak}{Ca} - d_0 k, \tag{3.25}$$

To facilitate the calibration it is possible to use the relationship between the force and the pressure ($p = \frac{f}{A}$) in Pa to generate the stimuli. The inverse transfer function in that case is:

$$p = \frac{\kappa\varepsilon_0 k}{Ca} - \frac{d_0 k}{A}, \tag{3.26}$$

The options for the approximation function are either a negative logarithmic function or a three to fifth order polynomial. Using polynomial approximation allows having robustness towards errors during the calibration process. Each individual tactile array requires calibration

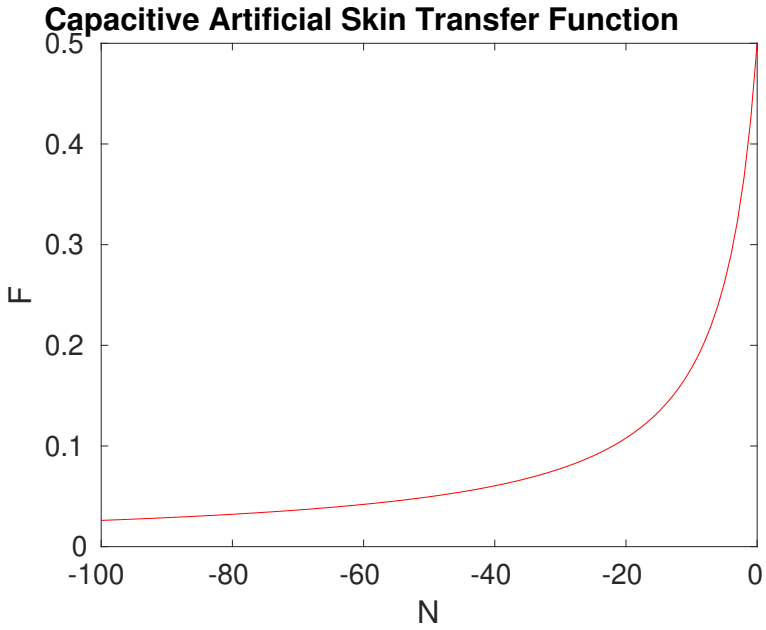

Fig. 3.10 Graphical representation of the transfer function.

and the resulting force can be taken from the sum of calibrated values. This allows to calibrate the artificial skin to retrieve the force measurements perpendicular to its surface, also called the normal force.

$$f_n = \sum_{t=1}^{N} f_t, \tag{3.27}$$

where f_n is the normal force in N, f_t is the force in the t-th tactile sensor in N, N is the number of tactile sensors in the array. This applies only for flat tactile arrays. Special considerations have to be made to calibrate curved surfaces.

To evaluate independent contacts an algorithm to group neighbor tactile sensors that have been activated is required.

3.4.2 Calibration Procedures

Methods covering tactile sensors force calibration can be roughly divided into two categories: individual sensor calibration and tactile surface calibration [66].

Individual sensor calibration

Some attempts have been made to calibrate the tactile sensors to estimate contact forces. One of the methods uses a technique that involves applying various forces mechanically on the

individual tactile sensors with a device that enables to measure the applied forces [100, 86, 68]. Therefore, it is possible to create the mathematical models that relate the applied force and the sensor values. However, all the methods that use this technique are very time-consuming, considering there can be hundreds of sensors within a single skin patch and each one of them has to be calibrated separately.

Multiaxis FT sensors measurements can be used to define a linear regression of the unknown local stiffness. Transformation matrices between the FT sensor and each tactile element are able to be calculated in the process [23]. This technique was conducted in a planar array of tactile sensors manually stimulating each tactile element, disregarding the gaps in between, and requires the FT sensors to exist on the robots which is not always the case.

Tactile surface calibration

Another technique applies uniformly distributed pressure on the skin to calibrate the skin [66]. The skin is placed inside a vacuum bag and the pressure is decreased inside the bag with a vacuum pump. The pressure and skin values are extracted during the experiment and the models, that relate pressure to the sensor reading, are generated for all the sensors simultaneously. The calibration takes only a few minutes and can be applied to a variety of skin shapes. The maximum calibration range is equal to the atmospheric pressure.

Based on a similar principle, a device was designed to perform the calibration procedure fast, accurately and with a very simple setup [65]. The pressure calibration range of this device is relatively large (3 bars) and can be used with skins of various shapes and sizes.

In all of the previously mentioned calibration techniques, the space between the tactile elements is neglected.

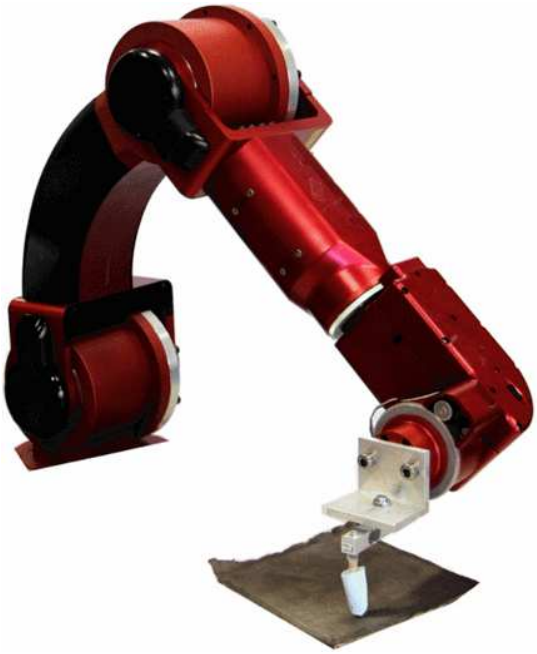

(a) Individual sensor calibration [100].

(b) Tactile surface calibration [66].

Fig. 3.11 Examples of artificial skin calibration.

3.5 Conclusions

Given the knowledge of how the senors are built and used, it is possible to realize how important force torque sensing is for robotics and what should a FT sensor accomplish. It is clear that there is room for improvement in the accuracy of contact force estimation. Six axis FT sensors have a long history in fixed base robots and they were sufficiently adapted to the way the were used, but the conditions and scenarios in floating base robots is very different. Even so, calibration and performance of commercially available sensors did not seem to adapt to these new requirements. Although artificial skin is a promising solution for estimation of force torque in multiple contact scenarios, it has not been fully used as a force torque sensor. The gap in between sensing elements is disregarded, but it might be possible to improve force estimation by taking them into account.The knowledge acquired in the field of force torque sensing generated a series of insights that motivated the research in this thesis.

3.5.1 Motivations

The main motivations of the presented research are:

- Given the dynamic equation of motion, eq.(2.1), the knowledge about contact forces and joint torques is fundamental for dynamic motions. Therefore studying how best to estimate these quantities is an interesting and relevant problem to solve. This information can be estimated with the aid of force-torque measurements.
- From the use of force-torque sensing in robotics is possible to see that force-torque sensors have a great potential already depicted theoretically. Therefore further improving this technology is valuable.
- Robots performance in real scenarios proves that in situations outside controlled environments the reliability of these sensors impacts greatly the performance of robots, especially floating base robots. The reliability of these sensors needs to be improved.
- A calibration procedure is fundamental for the reliability of a sensor since is what determines the performance of a sensor once the design is fixed.
- Knowledge of the working principles of the sensor and expected uses of it should guide the calibration procedure design.
- Tools to understand the validity of the calibration data can be very helpful in the calibration process and may also give useful insight in the behavior of the sensors.
- Mounting Force-torque sensors in mechanical structures like robots, affects their performance and besides the need to be calibrated at least once a year. Both issues can be addressed by *in situ* calibration procedures.
- The main technology used based on silicon semiconductor suffers from temperature drift. It should be taken into account in the sensors' calibration.
- Complex loading cases, drift and noise in the sensor ask for a comprehensive excitation of the sensor that could potentially consider dynamic modeling. To achieve this consistently might require a new *ex situ* calibration procedure.
- Six axis FT sensors, are able to sense the sum of forces and torques acting on a body, but struggle to independently identify different contacts. Other sources of force-torque sensing information should be explored.

Given the listed motivations, the objective of this thesis is to provide the knowledge and algorithms needed to have a reliable and accurate estimation of contact forces and joint torques exchanged between the robot, the environment and other objects. It focuses on improving the measurement reliability of the six axis FT sensors. This allowed robots to perform better

dynamical motions. This was achieved by developing novel *in-situ* calibration methods and proposing a new *ex situ* calibration device. Other sources of force-torque information, such as tactile arrays, were explored. This should enable the research community to better exploit force-torque sensing in complex structures such as robots.

3.5.2 Objectives

There are three intermediate goals to achieve the general objective previously described:

1. Deep understanding of force-torque (FT) sensors.
2. Improvement of force-torque sensors' performance.
3. Increase performance of dynamical motions in robots through the use of force-torque sensing.

To gain a deep understanding of the force-torque (FT) sensors the following actions were taken:

- Study the functioning principles of the different six axis FT sensing technologies.
- Understand how force-torque sensing is used in robots.
- Revise how force-torque sensing is used in robotics.
- Investigate how six axis FT sensors are usually calibrated.
- Develop tools for evaluating six axis FT sensors data.
- Analyze the performance of six axis FT sensors mounted on robots.

Seeking to improve force-torque sensors' performance the strategies implemented were:

- Development of *in-situ* calibration methods.
- Design of an improved *ex-situ* calibration method.
- Investigate the feasibility of using tactile sensors as force-torque sensors.

Aiming to increase the performance of dynamical motions in robots through the use of force-torque sensing, it was considered necessary to:

- Allow the articulated body to exploit the improved measurements.

- Evaluate the result of improving measurement quality.
- Allow the possibility to exploit other sources of force-torque information, such as tactile sensor arrays.
- Allow the robot to estimate individually forces when more than one force is acting on the same robot.

3.5.3 Assumptions

The thesis focuses mainly on six axis FT sensors and other possible sources of force-torque sensing. In regards to exploring six axis FT sensor behaviors on a robot and their *in situ* calibration, the research assumes the following:

- The model of the robot is known and considered accurate.
- The location of the sensors is known and the robot allows to excite the sensor in all six axis.
- The robot is able to be controlled to some extent without force-torque sensor feedback.
- An algorithm to exploit the measurements to estimate contact forces is implemented on the robot.
- The calibration matrix of the sensor is known. This is not strictly required.
- Ability to actually change the calibration inside the sensor is not required but is useful.

The other sources of force-torque sensing proposed are capacitive tactile sensor arrays. For these sensors the assumptions are:

- The sensor can be calibrated to measure either pressure or forces.
- The location of each individual taxel with respect to the robot is known or able to be calculated.

Chapter 4

Six Axis Force-torque Sensor Performance Evaluation Tools

Understanding the principles behind the sensors is important. But studying the actual behavior of the sensor mounted on a system can help understand how to more effectively improve the performance of the sensors. An easy fast way to evaluate calibration data is important for efficiency when doing sensor calibration. In this Chapter, methods for evaluating the performance of mounted six axis FT sensors are explained. The tools developed to obtain the evaluations are described. This is followed by a series of test to gain insights into the behavior of the sensors and their possible sources of error.

4.1 Performance Evaluation Tools

To analyze a sensor is crucial to be able to distinguish when a sensor is working correctly. To do this, a way to measure the performance of a sensor such that it allows a comparison between sensors is needed. To quantify the performance, a commonly used quantity is the Mean Square Error (MSE). Nonetheless, since the analysis was performed with mounted sensors on a robot is possible to create specially designed evaluation tools. Three tools for understanding and evaluating the sensors were designed. These tools were employed to gain insights into the performance of the available sensors. The tools are :

- Visualization Tool
- Sphere Analysis Tool
- Contact force validation Tool

4.1.1 Visualization tool

Experimental data can have unexpected behaviors. It is crucial to understand what could be the cause of the unexpected behavior. The visualization tool is meant to make this process much more intuitive and fast by providing a connection between the 3D space of either the forces or torques and the position of the robot at a certain point of an experiment. It uses the logged data of the experiment. It could be seen as a way to debug an experiment offline.

The visualization tool has two modes: one in which it runs the experiment as an animation and the other one in which is possible to select a specific sample of the experiment to analyze. It can receive an optional argument to plot the torques instead of the forces. The first mode allows also to record a video of the forces or torques. An example can be seen using the QR code in Fig. 4.1 or following this link. The second mode has some useful features for debugging an experiment:

- A slider to move along in the experiment.
- A text box in which a number can be entered to move the experiment to that specific sample.
- A button for saving a relevant sample and time of the experiment.
- A toggle button to select if the saved sample can be considered the beginning or end of an interesting section of the experiment.

Example of the visualization tool can be sin in Fig. 4.6. For the visualization of the iCub, the iDyntree [129] visualizer is used.

Fig. 4.1 Visualization video mode.

4.1.2 Sphere Analysis tool

Consider a body in which the center of mass does not change and is being moved in a spherical trajectory. When the body is moving slowly, such that acceleration of the body can be neglected, and no other force is acting on the body the only cause of force is the gravity. In this case, the magnitude of the force remains the same and what changes is the orientation with respect to the inertial frame. If we consider all the possible orientations then the gravity direction spans a unit sphere. This motion generates a sphere in the 3D force space where the radius of the sphere is mass times gravity ($m \times g$).

The sphere analysis tool uses this as a ground truth. By generating spherical motions with one of the limbs in which the FT sensor is mounted (an arm or a leg), an ellipsoid is fitted using the measurements of the sensor.

The radii of the ellipsoid correspond to the magnitude of the force when it is fully applied on the respective axis. If the sensor was perfect, the same value would be observed for the three force axis. Thus the difference between the among axes can be considered a value of their performance. The standard deviation (std) between the radii was selected as a performance index to represent the performance of a sensor with a single number. A value closer to zero

represents a better performance.
Furthermore, if the model of the robot can be trusted a reference sphere is generated to calculate what is the error in N of each force axis of the sensor. This can also be used to improve the fitting of the ellipsoid with the knowledge that we are expecting a sphere.

Using the sphere analysis tool a comparison can be made between the measurements of the sensor and the expected value. This is done by looking at how different the ellipsoid is from a sphere. An example can be seen in Fig. 4.2. It has been shown that this difference is related to a change in the effectiveness of the calibration and it can be corrected [130]. This difference can be considered a "deformation" of the calibration since an ellipsoid is considered a stretched (deformed) sphere.

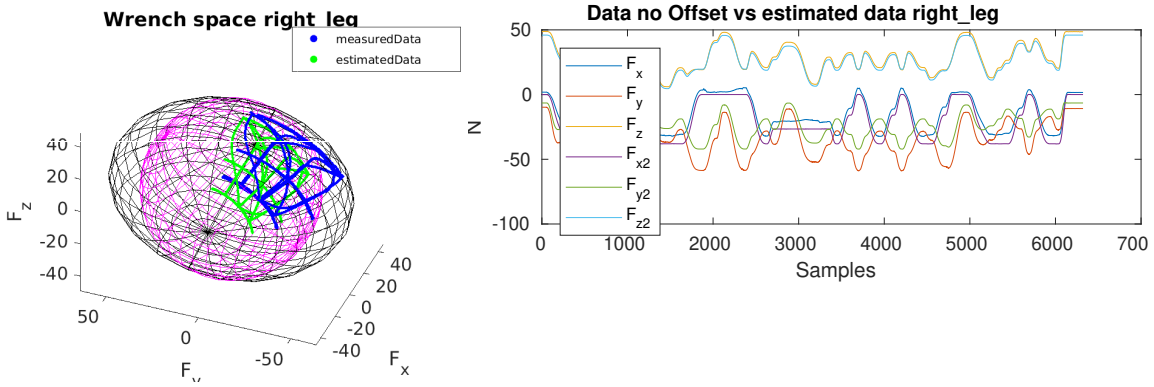

Fig. 4.2 Sphere Analysis Tool graphs.

In summary, we do the following:

- With the robot on the pole span a part of a sphere with the leg.
- Read force-torque measurements and kinematic information.
- Calculate the ellipsoid which fits the forces based in the sensor measurements.
- Obtain the radii of the ellipsoid and divide by gravity to obtain mass values.
- Calculate the std value.

If the model of the robot can be trusted then:

- Calculate expected wrenches at the force-torque sensor positions. To generate the reference sphere.
- Use reference sphere to improve the fitting of the ellipsoid.

- The center of the fitted ellipsoid is considered the offset and can be easily removed.
- Compare mass values or forces as a measure to know how accurate the measurements were.

When the model can not be trusted, it is possible that a sensor has a low std value, but its measurements are not reasonable. For example, if a sensor has a perfect sphere of 70 N radii when the load applied is something around 50 N. Nonetheless, it might mean that the sensor itself is less prone to deformation due to mounting. In this case, the results of the tool give us mainly an insight into the coherence of the sensor with regards to its calibration.

4.1.3 Contact Force Validation

This evaluation tool reproduces offline the behavior of the contact force and joint torque estimation of the robot described in Section 2.4. It simulates the behavior of a sensor as if it was being used by the robot and allows to quantify its performance. In the estimation scheme, the robot is divided into sub-models by cutting the robot in locations where a FT sensor is found. The contact force validation procedure consists of estimating the contact forces in a sub-model where no contact or contact force is experienced. The value of the estimated contact force should be zero. An example of such sub-model in the iCub can be found between the sensor at the hip and the one at the ankle.

The contact 6D force value is estimated at a given contact point. Then, is brought back to the sensor frame being analyzed at the moment. By applying :

$$\mathrm{f}^{s} = {}_{s}X^{k}\mathrm{f}^{k} \tag{4.1}$$

where ${}_{s}X^{k}$ is the transformation matrix from the contact point to the sensor, f^{k} is the 6D force vector at the contact frame and f^{s} is the 6D force vector at the sensor frame. This way it is possible to know the contact force measured by an axis of the sensor.
The performance evaluation can be done on the magnitude of the force and in each axis separately. When we use the evaluation on the magnitude, it allows to evaluate the performance of a calibration matrix as a whole. Instead when looking at each axis as a separate evaluation, it is possible to measure a calibration matrix performance of that axis.
The estimation scheme combines the information of the sensors found in the sub-model. At any given time of the contact forces estimation, just one calibration matrix is being evaluated, even if the tool itself evaluates more than one sensor and multiple calibration matrices for that sensor in a single run. It has two modalities based in the source of the information of the other FT sensors involved in a sub-model. The first mode uses the estimated wrenches using only the

model for all sensors except the one being evaluated at the moment. The second mode uses the logged measurements of all sensors except the one being evaluated at the moment.
The first modality allows for a cleaner evaluation of the sensor since we are using ideal estimation values for the sensors not being evaluated. This modality is restricted to the fact that the estimation wrenches are only accurate when there is only one contact on the robot. The second modality is able to evaluate a general performance of the robot as long as the sub-model in which is being tested has no contact, but it might suffer from the errors in the measurements of the other sensors. This performance tool was mainly used to select a calibration matrix that had the best results on improving the performance of the robot.

4.2 Application

4.2.1 Comparison of sensors mounted in the Robot

Using the Sphere Analysis Tool provides an objective way of quantifying the performance of a sensor. This allows comparison between sensors even when the experiment data is taken at different times. In here, we enclose just a small representative subset of the sensors that were evaluated.

Description of sensors used in the comparison

There were mainly three kinds of sensors to compare: the FTsense strain 1, FTsense strain 2 and the ATI mini 45. The characteristics of these sensors are described in A.2.1. The naming convention for the FTsense is SNXXX, where 'SN' referrs to 'serial number', and 'XXX' is the actual serial number.

FTsense strain 1 sensors:

- SN138 : mounted on right leg of iCubGenova01
- SN140 : mounted on right leg of iCubDarmstadt01
- SN269 : mounted on right leg of iCubGenova04
- SN233 : mounted on left leg of iCubDarmsdtadt01
- SN106571[1] : mounted on left leg of iCubGenova01.

[1]The SN106571 is a slightly modified version of the strain 1. It has a spine that prevents displacement in the inner mechanics of the sensor once it is closed. This sensor loses its advantage if it has to be reopened for any reason.

FTsense strain 2 sensors:

- $SN282_{insitu}$: mounted on the right leg of iCubGenova04, using the calibration estimated in situ [2].
- SN282 : mounted on the right leg of iCubGenova04
- SN234 : mounted on the right leg of iCubGenova02
- SN233 : mounted on the left leg of iCubGenova02

The ATI mini 45 : temporarily mounted on the right leg of iCubGenova04.

For the sensors FTsense strain 2 and the ATI more than one data set was collected. Only the first and last test are presented.

Test description

In summary, the steps are the following:

- With the robot on the pole run a spherical grid movement on a chosen leg.
- No contact forces should be applied during the grid movement.
- Read and record force-torque measurements and kinematic information.
- Evaluate the degree of deformation of the sensor's calibration using the sphere analysis tool.

Results

The performance of the sensor is evaluated with regards to the std value calculated on the three force axis. From the performance analysis in Table 4.1, it can be concluded that mounting a sensor in the robot does change its performance. An example can be seen in Fig. 4.3. The performance of the ATI is less affected by the mounting procedure as it can be seen from Fig. 4.4. Sensors with a performance index (std) below 0.6 were rare. In comparison to the average sensor, the in situ calibrated sensor had a std value 4 to 10 times smaller. Thus, the best performance is from the FTsense strain 2 using the in situ calibration.

The modified version of the FTsense strain 1, did not seem to have any particular advantage, although the deformation of the calibration in the torque axis was not tested. It can also be

[2] The in situ calibration method is described in Chapter 5 with no temperature compensation

observed for the sensors with multiple tests that the sensors are affected by drift as seen in Table 4.1.

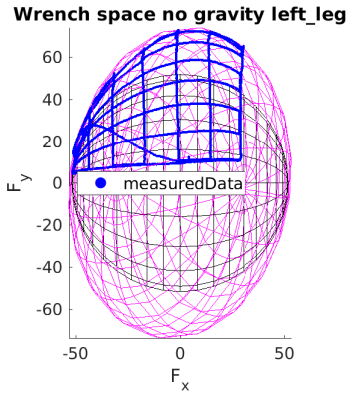

(a) x-y plane no reference

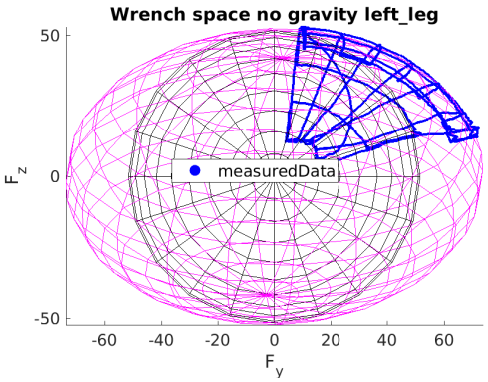

(b) y-z plane no reference

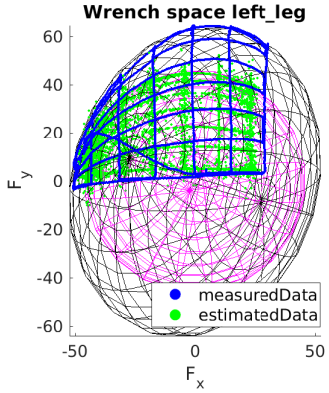

(c) x-y plane with reference

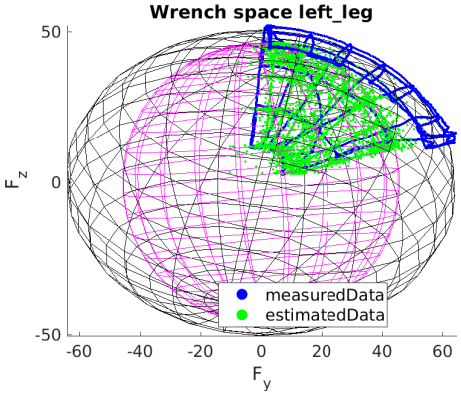

(d) y-z plane with reference

Fig. 4.3 Example of calibration deformation on sensor SN333.

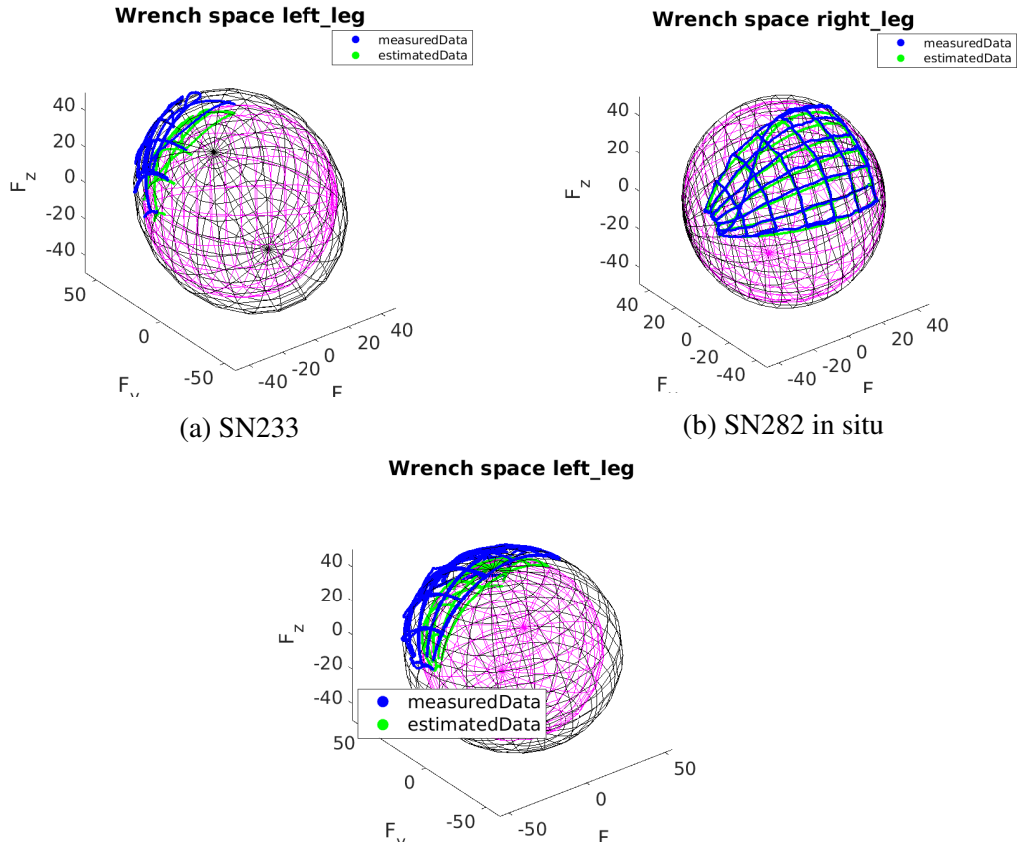

(a) SN233

(b) SN282 in situ

(c) ATI mini 45

Fig. 4.4 Sensors with best performance from each kind

4.2.2 Using Visualizer for Identification of troublesome joint configurations

After an experiment with the sensor SN282, some unexpected behavior of the forces was observed as showed in Fig. 4.5 and Fig. 4.6. This was also confirmed with the Sphere Analysis Tool, by having a std value out of the average when not using the reference as seen in Table 4.1.

By using the visualization tool, it could be observed that reaching the joint configurations in Table 4.2 created the unexpected behavior. After looking at the posture and retrieving the joint configurations (using the sample number at which the behavior was observed), it was possible to replicate the configuration on the robot and verify if the behavior was repeatable.

The reason was found to be that the robot was touching the covers generating an undesired contact force. This allowed to change the sequence to avoid the issue in the future and avoid using the data of the periods of the experiment were the undesired contact forces were observed. The data of the experiment with those sections removed is showed in Fig. 4.7.

	With Reference				No Reference
Sensors	Error x	Error y	Error z	Std	Std
SN169	5.9484	24.5433	2.6872	1.2019	0.9024
SN140	9.5884	15.1658	1.6366	0.6931	0.7998
SN138	−6.5550	17.4981	2.5578	1.2379	0.5249
SN233	2.2601	11.4800	2.4087	0.5383	0.5225
SN106571	19.1296	15.0756	2.7308	0.8707	1.0892
$SN333_1$	5.8339	17.7120	4.1286	0.7543	1.3778
$SN333_2$	5.6101	18.7182	4.2647	0.8139	1.3158
$SN334_1$	7.5575	19.7817	4.5297	0.8231	1.0713
$SN334_2$	8.5443	19.1929	4.3815	0.7787	1.0669
$SN282_1$	9.1065	26.9490	7.0502	1.1155	2.4238
$SN282_2$	9.0371	25.5854	6.4697	1.0576	2.1551
$SN282_{insitu_1}$	0.4174	1.6623	2.7594	0.1194	0.3896
$SN282_{insitu_2}$	0.8401	1.5680	3.3363	0.1309	0.6307
ATI_1	8.0796	15.3603	3.1578	0.6258	0.1828
ATI_2	8.2997	14.6807	5.3031	0.4882	0.2400

Table 4.1 Sphere Analysis Tool results.

'r_hip_pitch'	'r_hip_roll'	'l_hip_pitch'	'l_hip_roll'
−28.3995	6.0040	−28.4382	5.9985
−30.0202	72.8011	−30.0202	72.7956
−12.1784	75.4378	−12.2221	75.5202
5.3119	72.6693	5.3119	72.6198
40.8198	74.0757	40.7319	74.0698
58.3101	75.7894	58.3980	75.7839
76.0640	73.2405	76.0640	73.2350
−28.6140	6.0040	−28.7897	5.9985

Table 4.2 Identified joint configurations with unexpected behavior

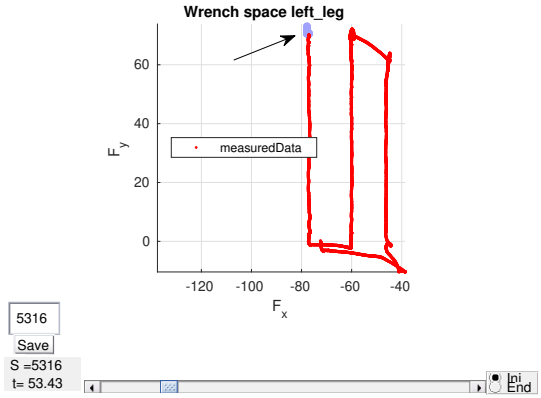

(a) x-y plane of force visualizer

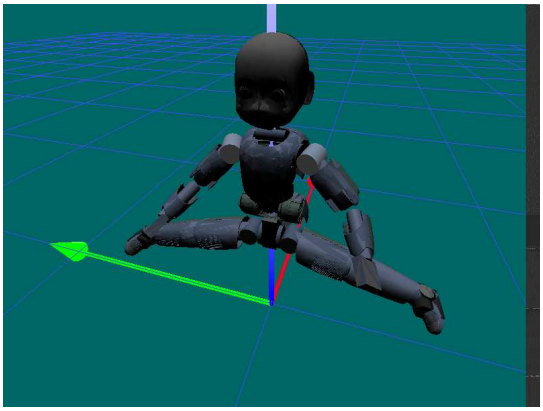

(b) Robot visualizer

Fig. 4.5 Reaching 73^o in the hip roll

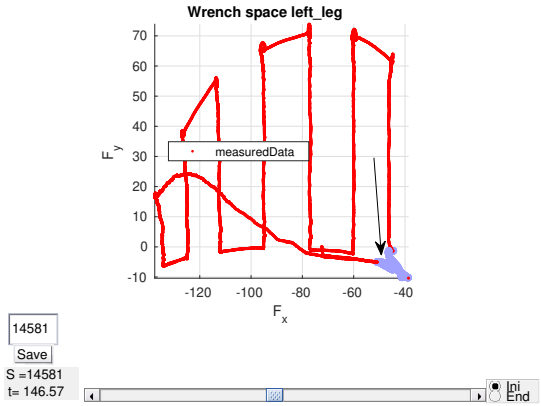

(a) x-y plane of force visualizer

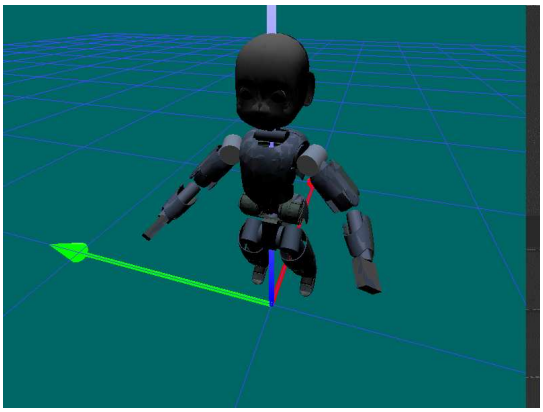

(b) Robot visualizer

Fig. 4.6 Reaching -28.4^o in the hip pitch

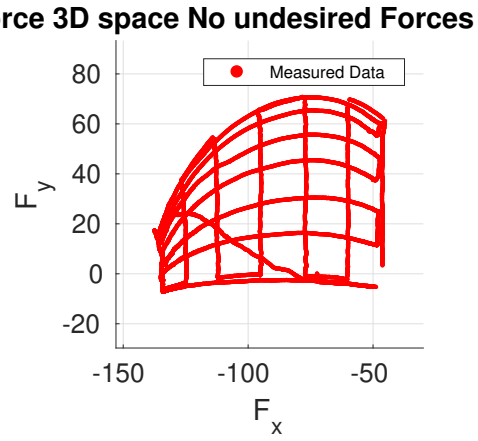

Fig. 4.7 Data experiment with sections removed

4.2.3 Mounting tests

A change in the behavior of a sensor has been observed after mounting [130]. In an attempt to understand the reason for this change, some tests regarding the mounting of the sensor were designed.
The tests performed were related to the value of the torque used when screwing the sensor into the robot. The idea is to see if these torque values affect the sensor and if there is a strategy to minimize the change in behavior. The test steps were defined as:

- In the first iteration, do not change the torque on the screws. In the next iterations progressively reduce the value of the torques starting from 2 Nm.
- Run a spherical grid movement on a chosen leg and record the data.
- No contact forces should be applied during the grid movement.
- Evaluate the degree of deformation of the sensor's calibration using the sphere analysis tool.
- Loose the screws in one leg and repeat the experiments.
- Compare with results obtained from other experiments with different torque values.

Data sets and remarks

Six cases where considered. The cases are: 2 Nm, 1.5 Nm, 1 Nm, 0.5 Nm, 1 Nm on x-axis screws 2 Nm on the others (mixed1-2 Nm), 2 Nm on the x-axis screws 1 Nm on the others (mixed2-1 Nm). The screws aligned with the x-axis can be seen in Fig. A.5. In the figure,

x-axis is pointing to the right of the third image.
For most of them 4 datasets were taken on the right leg of the iCub. Using 2 Nm to screw the sensor seemed to be already at the limit of the screw. Due to some problems with a cable being crushed under some positions of the robot during the execution of the spherical motions, only the 2 Nm datasets where done in the left leg before changing to the right leg. Also, one dataset of the 1 Nm test was incomplete due to issues with the logging application.
At the moment of the tests, the iCub had not been fine-calibrated, so there is no guarantee the calculated wrenches were correct. Therefore the reference sphere generate was created using the smallest radii for easier visual inspection.

Results

Best results according to the Sphere Analysis tool, where achieved on the left leg when the screws were all on 2 Nm shown in Fig. 4.8, followed close by the right leg all screws at 1 Nm. Both of these sets have a sample with 0.5 as std value which is by far outliers w.r.t the general obtained values in all other tests. The resulting std values obtained in the experiments are shown in tables 4.3 and 4.4 . Fig. 4.9 shows the worst performance for comparison.

From the results it could be seen the following observations:

- The std value when different torques where used to screw was higher than using the same torque to screw the sensor. Therefore, a unique torque values to screw the sensor to the robot improves the performance.
- Leaving the screw too loose or having different torque values in the screws generates a higher std value than the one calculated on the ex situ calibration data. This means these scnearios decrease the performance of the sensor.
- Leaving the y-axis more loose has higher std value than leaving the y-axis more loose. So the axis more susceptible to deformation is the y- axis.
- The values that have the best performance are 2 Nm and 1 Nm. This is unexpected since 1 Nm was already below the suggested minimum of the screw which was 1.4 Nm.
- Even having the same value for all screws does not make the performance of the sensors comparable to the one seen with the ATI or the in situ calibrated sensor in subsection 4.2.1.

-	Original	2 Nm
First Trial	1.0090	0.5272
Second Trial	-	0.7245
Third Trial	-	0.8738
Fourth Trial	-	0.7123
Average Std	-	0.7095

Table 4.3 Table comparing std of the experiments on the left leg.

-	Original	1.5 Nm	1 Nm	0.5 Nm	mixed1-2 Nm	mixed2-1 Nm
first Trial	1.0935	0.8974	0.5778	1.0717	0.7938	1.1639
second Trial	-	0.8789	-	1.0893	0.7739	1.0797
third Trial	-	0.9156	0.7143	1.0908	0.8774	1.0860
fourth Trial	-	0.9620	0.8389	1.1203	0.8972	1.1283
average Std	-	0.9135	0.7103	1.0930	0.8356	1.1145

Table 4.4 Table comparing std of the experiments on the right leg.

In Appendix B are reference images to appreciate the deformations found in the different experiments. For a common reference, the third trial was taken from each set.

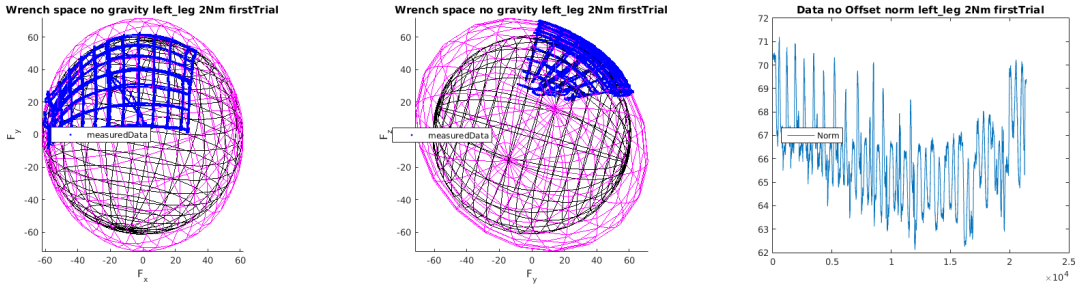

(a) x-y plane (b) y-z plane (c) Norm over samples

Fig. 4.8 iCubGenova04 robot sensors ellipsoids, best results

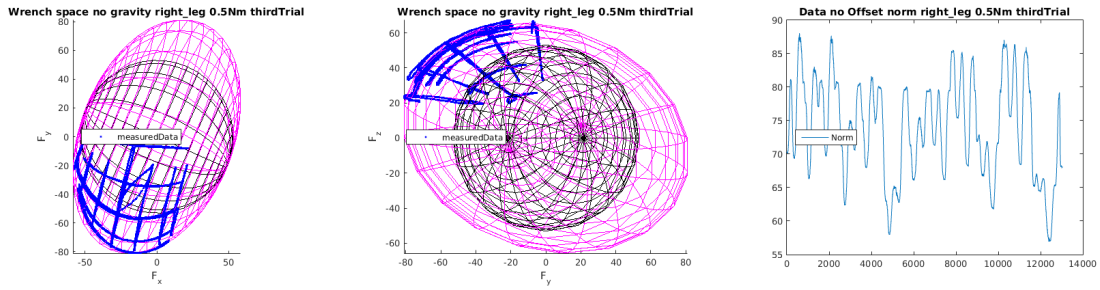

(a) x-y plane (b) y-z plane (c) Norm over samples

Fig. 4.9 iCubGenova04 robot sensors ellipsoids, right leg 0.5Nm experiments

4.2.4 Conclusions

Mounting a sensor on the robot makes less effective the calibration of the sensor. Having the same value on all screws seems to help avoid having some deformation on the calibration of the sensor, but it does not solve the problem. There also does not seem to be a correct unique value for screwing but seems something between 2 Nm and 1 Nm is fine. The important thing is to have the same torque in all screws. Having the chosen value close to 2 Nm might be preferable. Depending on the type of screw used it might be possible that 2 Nm is a value to close to the limit of the screw. This has to be taken into consideration.
It seems important to notice the biggest deformations were in the big majority of cases in the y-axis.

Multiple tests on the same sensor have shown a degrade in the performance of the sensor. This is due mainly to drift and affects the measurements. Due to this phenomena it is a common practice to re-estimate the offset or bias of the sensor before starting an experiment.

The use of a calibration estimated in situ shows a big improvement with respect to the other sensors.

4.3 Problems Observed in Silicon Based Force-torque Sensors

Given the results and experience working with the sensors, five main issues were identified. This problems prevent to fully trust the measurements of the FT sensors on the robot.

4.3.1 Calibration change after mounting

FT sensors are prone to change performance once mounted in a mechanical structure such as a robot [130, 8]. The Tables 4.1, 4.3 and 4.4 corroborate this behavior. This issue has motivated the creation of in situ methods to re-calibrate the sensor in its final destination. The reason behind this change has not been fully studied. It could be seen in Section 4.2.3, that the torque with which the sensor is mounted does affect the measurements, but is not the only cause. Other sources of this problem could be in the machining of the sensor and the sensor interfaces.

4.3.2 Saturation

Saturation in the sensor arises from the ADC reaching its limit in any of the six channels of the sensor. The behavior of the sensor, when saturated, is to send a saturation message and keep streaming the last valid values before saturation. On the iCub this logic is temporarily

lost in the upper levels where in case of saturation the data is simply not streamed in the ports, but when using the implementation of the estimation scheme in 2.4 on the robot any not-ok force-torque measurements, including saturation, are taken care differently.
The behavior is the following:

- If the measurement is not ok, then the previous measurement value is not replaced.
- Therefore the previous value will be reused in the estimation of joint torques and contact forces.
- The low-level controller receives constant values.

An example of how a saturation looks from the forces and torques perspective can be seen in Fig.4.10a. The actual saturation is much better appreciated when looking at the raw data since the actual saturation happens at the channel level. An example of this can be seen in Fig. 5.8a In the case of the FTsense strain 1, this was a very serious issue creating problems in the controller. The gain selection feature in the FTsense strain 2 allows to overcome this by selecting the right gains.

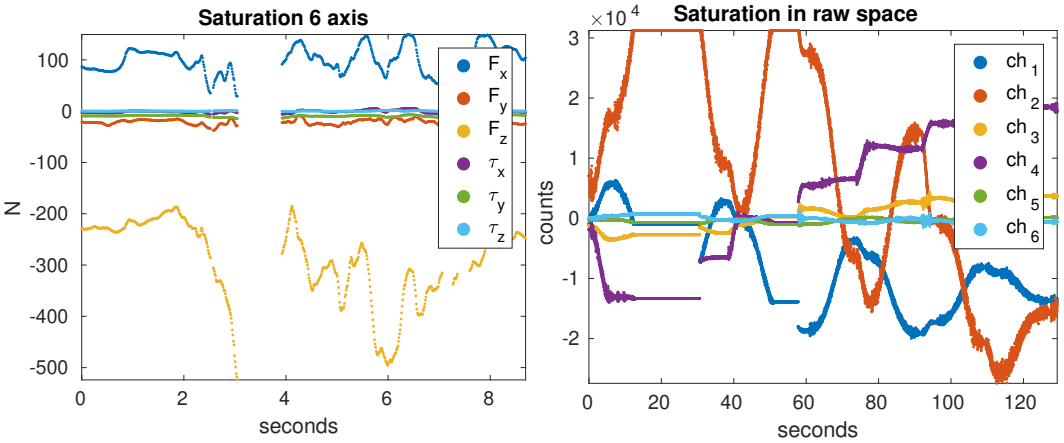

(a) Saturation of sensor in FT values

(b) Saturation of sensor in Raw values

Fig. 4.10 FT sensor behavior when suffering saturation.

4.3.3 Temperature Drift

The FTsense Strain 2 includes a temperature sensor. This allows to study the effect of temperature in the measurements. A common solution to compensate temperature effects when using strain gauges is to use the Wheatstone bridge circuit to compensate for temperature [57]. But this method is effective to compensate for temperature only if all strain gauges are subjected to the same temperature change. Given the dimensions and arrangement of the strain gauges

inside the FTsense, applying this method to compensate for temperature was not feasible when the sensor was designed. To observe the effect of temperature on the measurements, a heat gun was used to heat a F/T sensor while measuring the load of a 33 kg robot. The initial load is removed to show the change in measurements caused by the change of temperature. The temperature effect is clearly visible on the z-axis, which is the one experiencing most of the load as shown in Fig. 4.11a. The effect of temperature looks close to a linear behavior. The temperature also affects the other axes as shown in Fig. 4.11b and Fig. 4.11c. The temperature seems to affect more the forces than the torques. The observed vibration while heating up was induced by the air coming from the heat gun. The effect of temperature hysteresis can also be appreciated in the figures.

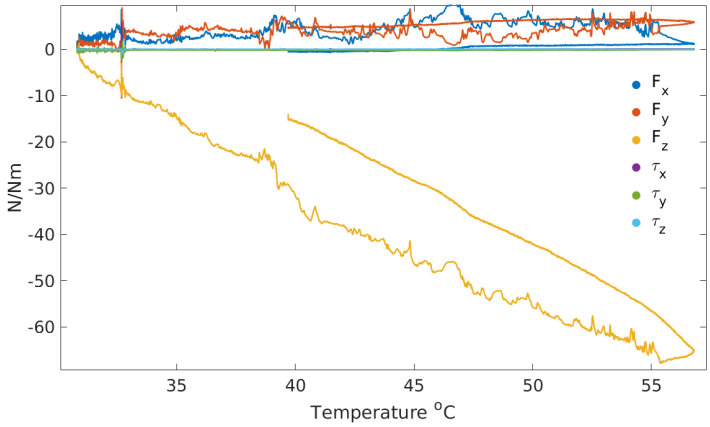

(a) Temperature effect

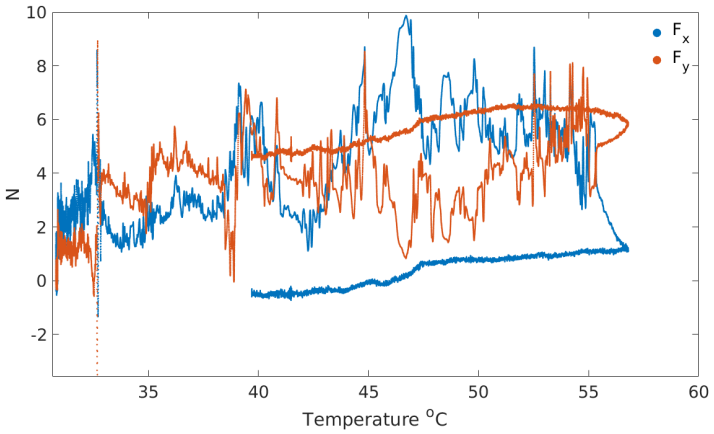

(b) Temperature effect on F_x an F_y

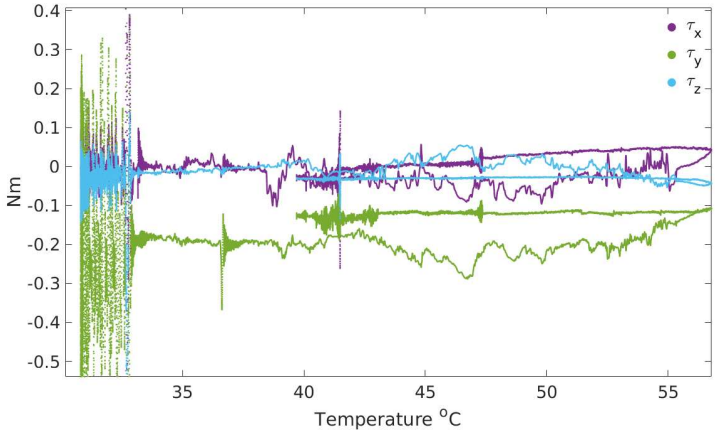

(c) Temperature effect on Torques

Fig. 4.11 Temperature effect on the FT measurements

4.3.4 Full Scale calculation

The current full scale information that appears on the FTsense is based on the maximum value obtained by having saturated values in all channels. This becomes an unrealistic value since the sensors will stop streaming new values as long as one channel is saturated. Given the observed behavior of the raw data of the sensors, it is very unlikely that there will be a case where all channels saturate at the same time as observed in Fig.5.8a. As a result, the limit value specified by the full scale is much higher than the actual values that can be achieved through the usual use of the sensor.

4.3.5 Offset variability

While the higher unit resistance and sensitivity of silicon-based gauges are definite advantages, their greater sensitivity to temperature variations and tendency to drift are disadvantages as mentioned in Section 1.3.1. This plus the effect of hysteresis may result in a different offset value for each experiment, but it is assumed the offset remains constant during the experiment due to the small time frame of each experiment. The effects of drift and hysteresis are currently not considered in the model. This also means that the offset estimation should be done before every experiment. It reduces the reliability of the sensors over a longer period of time.

4.4 Conclusions

Even if the decrease in performance due to mounting can be mitigated by using an specified torque value to screw the sensor, it is considerable. The decrease in performance in repeated experiments shows the consequences of drift. Temperature drift is not negligible. A way to minimize its impact is desirable. The saturation problem can be solved by selecting the gains of the ADC converter based on experimental data. Calibration change, temperature drift and offset variability can be tackled with a proper *in situ* calibration. This is addressed in Chapter 5.